

THESIS

SNOWPACK DEPLETION MODELING USING FAST ALL-SEASON SOIL
STRENGTH (FASST) AND SNOWMODEL IN A HIGH-ELEVATION, HIGH RELIEF
CATCHMENT IN THE CENTRAL ROCKY MOUNTAINS

Submitted by

Anne Elizabeth Sawyer

Department of Forest, Rangeland, and Watershed Stewardship

In partial fulfillment of the requirements

For the Degree of Master of Science

Colorado State University

Fort Collins, Colorado

Summer 2007

ABSTRACT OF **THESIS**

SNOWPACK DEPLETION MODELING USING FAST ALL-SEASON SOIL STRENGTH (FASST) AND SNOWMODEL IN A HIGH-ELEVATION, HIGH RELIEF CATCHMENT IN THE CENTRAL ROCKY MOUNTAINS

In the western United States, snowmelt from mountain basins has historically provided 70-90% of annual runoff and the winter snowpack acts as a reservoir to store water for spring and summer soil moisture and stream recharge. Modeling the timing and magnitude of snowpack depletion and runoff in mountainous basins is an essential tool for forecasting water supply for irrigation, drinking and industrial uses. Modeled point estimates of snow depth depletion at two forested, sub-alpine sites (using Fast All-Season Soil Strength (FASST) and SnowModel) were compared to observed seasonal snow depths from an acoustic snow depth sensor. Meteorological forcing data for each model were collected at both sites between March and June of 2003 and included air temperature, relative humidity, air pressure, wind speed and direction, incoming and outgoing shortwave radiation and upwelling and downwelling longwave radiation. Precipitation was measured using precipitation gauges near each site.

SnowModel was also used to simulate distributed snow cover depletion and runoff in a mountain catchment, St. Louis Creek (82.5 km²), at varying spatial resolutions of Hydrologic Response Units (HRUs). HRUs were created based on physiographic characteristics of the basin including elevation, slope, aspect and vegetation cover. The number of HRUs in five simulations ranged from one (basin average) to 3726. Snow-

covered area (SCA) and basin-average snow water equivalent (SWE) depletion curves were generated for each simulation. Depletion curves were compared to modeled and observed St. Louis Creek discharge. Diversions above the basin outlet necessitated the reconstruction of 2003 St. Louis Creek discharge using statistical relationships between discharge from St. Louis Creek and two smaller gauged streams within the basin using pre-diversion discharge data (1943 – 1955).

Both FASST and SnowModel successfully simulated one-dimensional snow depth depletion at both sites when compared to observed snow depth using standard statistical metrics for evaluation. SnowModel produced realistic SCA and SWE depletion curves for St. Louis Creek basin, and the finest spatial resolution simulation best represented the spatial variability within the basin and produced the most realistic results. However, as anticipated, the timing and magnitude of runoff was incorrect due to a lack of a runoff routing module within SnowModel.

Anne Sawyer
Department of Forest, Rangeland, and Watershed Stewardship
Colorado State University
Fort Collins, CO 80523
Summer 2007

ACKNOWLEDGEMENTS

First and foremost, this project was made possible through the support and encouragement of my primary advisor, Kelly Elder. In addition to providing me with a project and academic insight, Kelly provided opportunity for field work, encouraged my ski career, and was incredibly supportive through challenging times.

I'd also like to thank my co-advisor, Steven Fassnacht, for his encouragement, ideas, and patience. This project would not have been completed without assistance from Glen Liston, whom I'd like to thank for his ideas and his patience. Thank you to Susan Frankenstein for her help with SNTHERM and FASST and Greg Butters, both of whom were on my committee. I'd very much like to thank Laurie Porth, USFS Statistician, who helped me reconstruct St. Louis Creek discharge. Other people who contributed to this work include Elke Ochs, Chris Heimstra and Gus Goodbody.

This project was funded by the US Army Corps of Engineers -- Cold Regions Research and Engineering Laboratory (CRREL), with special thanks to Robert Davis. NASA Cold Land Processes Field Experiment (CLPX) (Don Cline, PI) provided funding for data collection.

Perhaps most importantly, I'd like to thank my mother. Thanks also to my dad and Aunt Jeanie and Uncle Rich in Fort Collins. A huge thank you my friends in Fort Collins, particularly Lindsay Reynolds and Abby Korte. This work is dedicated to my Grandmother Betty and my Great Aunt Theresa. You are both tremendously missed.

TABLE OF CONTENTS

ABSTRACT OF THESIS	iii
ACKNOWLEDGEMENTS	v
TABLE OF CONTENTS	vi
1. INTRODUCTION	1
2. BACKGROUND	3
2.1 DISTRIBUTED SNOWMELT MODELING	3
2.2 SNOW-COVERED AREA DEPLETION CURVES	7
2.3 MODEL APPLICATIONS	9
2.3.1 FAST ALL-SEASON SOIL STRENGTH (FASST)	9
2.3.2 SNOWMODEL	9
3. OBJECTIVES	12
4. STUDY AREA	14
5. MODELS	17
5.1 FASST	17
5.2 SNOWMODEL	21
5.2.1 MICROMET	22
5.2.2 ENBAL	26
5.2.3 SNOWPACK	27

6. DATA AND METHODS	29
6.1 POINT SIMULATIONS	29
6.1.1 METEOROLOGICAL INPUTS	29
6.1.2 SOIL	32
6.1.3 FASST INITIALIZATION	32
6.1.4 SNOWMODEL INITIALIZATION	33
6.2 POLYGON SIMULATIONS	34
6.2.1 TERRAIN SEGMENTATION AND AGGREGATION	34
6.2.2 TOPOGRAPHIC AND LAND COVER DATA	35
6.2.3 SLOPE, ASPECT AND ELEVATION	35
6.2.4 VEGETATION	40
6.2.5 METEOROLOGICAL INPUTS	43
6.2.6 INITIAL SNOW WATER EQUIVALENT DISTRIBUTION	45
6.2.7 SNOWMODEL SIMULATIONS	45
6.2.8 ALBEDO SENSITIVITY ANALYSIS	47
6.3 ST. LOUIS CREEK DISCHARGE RECONSTRUCTION	49
6.4 SNOW-COVERED AREA DEPLETION CURVES	54
6.5 STATISTICAL ANALYSES OF POINT MODEL RESULTS	54
6.6 STATISTICAL ANALYSES OF DISTRIBUTED MODEL RESULTS	55
7. RESULTS AND DISCUSSION	56
7.1 POINT SIMULATIONS	56
7.1.1 FOOL CREEK	56
7.1.2 ST. LOUIS CREEK	59

7.2 POLYGON SIMULATIONS	62
7.2.1 SNOW WATER EQUIVALENT DEPLETION	62
7.2.2 SNOW-COVERED AREA DEPLETION	69
7.2.3 BASIN AVERAGE TEMPERATURE	75
7.2.4 ST. LOUIS CREEK RUNOFF	76
7.2.5 SNOWMODEL RUNOFF	78
7.3 COMPARISON OF POLYGON RESULTS TO METEOROLOGICAL TOWER DATA	81
7.3.1 PRECIPITATION	81
7.3.2 AIR TEMPERATURE	82
7.3.3 RADIATION	83
7.4 PRECIPITATION CORRECTION	84
8. CONCLUSIONS	89
9. REFERENCES	92

CHAPTER 1. INTRODUCTION

Water from melting snow is a critical resource in many mid-latitude regions of the world. In the western United States, snowmelt from mountain basins has historically provided 70-90% of the annual runoff and the winter snowpack acts as a reservoir to store water for spring and summer delivery to soils and streams (Doesken and Judson, 1997). The spatial distribution of snow in mountainous basins can affect the spring-snowmelt timing, magnitude and spatial variability (Luce *et al.*, 1998). Watersheds in mountainous areas are characterized by extreme variations in topography, vegetation, soils, climatic conditions and snow cover distributions, and the high spatial variation in these areas needs to be considered when modeling hydrological processes in alpine basins (Gurtz *et al.*, 1999). Distributed snowmelt models attempt to incorporate spatial variability of the land surface and meteorological processes and allow fundamental representations of the hydrological processes within a watershed (Kouwen *et al.*, 1993). Successful examples of distributed snowmelt models are prevalent in the literature (e.g. Leavesley and Stannard, 1990; Harrington *et al.*, 1995; Cline *et al.*, 1998; Link and Marks, 1999; Luce and Tarboton, 2004; Thyer *et al.*, 2004) with most requiring detailed meteorological input that may or may not be available. Additionally, the spatial scale needed to accurately model basin processes can vary significantly, and can be much larger than the process scale (e.g. Wood *et al.*, 1988; Famiglietti and Wood, 1995; Cline *et al.*, 1998).

This study investigated the spatial scale of snowmelt modeling in a mountainous, mid-latitude basin in north-central Colorado using SnowModel, a distributed snow evolution modeling system (Liston and Elder, 2006a) to predict snow cover depletion rate and timing as affected by varying physiographic characteristics. Additionally, point model estimates of snow depth using SnowModel and Fast All-Season Soil Strength (FASST) (Frankenstein and Koenig, 2004) were used to evaluate the performance of both models in this environment.

CHAPTER 2. BACKGROUND

2.1 DISTRIBUTED SNOWMELT MODELING

Distributed snowmelt models attempt to quantify processes in snow covered environments that cover a variety of space-time scales by parceling the catchment into a number of modeling units that assume uniform parameters and processes within each unit. A computational unit may be either a hydrologic response unit (HRU), which is based on a homogenous response to meteorological stimuli, or for convenience, square grid-based elements (Kirnbauer *et al.*, 1994). HRUs represent areas having homogenous hydrologic response according to the most important factors controlling runoff, such as amount and type of meteorological inputs, topography (e.g. elevation, slope, aspect), land cover and soil characteristics (Gurtz *et al.*, 1999). The critical assumption regarding HRUs is that variation within an HRU must be small when compared to variation between HRUs (Flügel, 1995). HRUs may be grid-based (e.g. Flügel, 1995; Battaglin *et al.*, 1996; Gurtz *et al.*, 1999) but polygon-based modeling (e.g. Leavesley and Stannard, 1990; Kite and Kouwen, 1992; Becker and Braun, 1999) has the advantage of directly representing the natural drainage structure of the land surface (Becker and Braun, 1999).

Hydrological models are applied to individual HRUs or aggregations of contiguous or non-contiguous HRUs that exhibit equal hydrologic behavior (Gurtz *et al.*, 1999) regardless of their size, form and spatial pattern (Becker and Braun, 1999). The

number of HRUs required to adequately represent basin characteristics varies with individual basins. Regions with highly heterogeneous terrain and land cover, such as alpine basins, likely need more HRUs than regions with homogeneous terrain, such as prairie environments (Kite and Kouwen, 1992). Additionally, the spatial scale of modeling units can impact results, with greater spatial scales resulting in a loss of explicit information, such as the exact distribution of snow or snow water equivalent in a basin (Cline *et al.*, 1998). However, at some larger modeling scales the influences that individual basin characteristics exert on hydrological response may attenuate, and sufficient representation of basin response can be achieved with significantly less knowledge of underlying basin physical characteristics. This critical scale is known as the Representative Elemental Area (REA) (Wood *et al.*, 1988).

It is essential, particularly in heterogeneous alpine basins, for snowmelt models to account for much of the variability in energy and mass fluxes as a function of terrain and land cover. Charbonneau *et al.* (1981) estimated that the effects of orientation and shading in mountainous terrain could locally modify the energy budget for snowmelt by more than 100%. Increases in precipitation and snow water equivalent (SWE) as well as decreases in air temperature and changes in processes controlled by air temperature, such as turbulent heat transfer and the transition of rainfall to snowfall are all dependent on elevation. Slope and aspect alter the amount of radiation received by the surface and affect predominant wind direction, resulting in heterogeneous distribution of snow cover throughout the basin (e.g. Meiman, 1968; Charbonneau *et al.*, 1981; Blöschl *et al.*, 1991). Variations in vegetation cover are also known to have large effects on rate and quantity of melt production due to vegetation altering the mass and energy flux near the snow

surface (Metcalf and Buttle, 1995). All of the above factors influence the energy exchange at the snow surface, which governs the production of meltwater. Radiative flux is generally considered to be more important than the turbulent exchange process, although the turbulent flux can have considerable impact on melt due to its ability to assist or counteract the radiative flux (Male and Granger, 1981). Modeling snowmelt using the HRU concept attempts to account for these variations in energy flux at the snow surface.

Leavesley and Stannard (1990) conducted a study using the United States Geological Survey's (USGS) Precipitation-Runoff Modeling System (PRMS) to model runoff and snowmelt in an alpine basin in the Sierra Nevada. The disaggregation of the basin into HRUs was accomplished by first dividing the basin into subwatersheds, and subwatersheds into two opposing hillslopes. The average slope, aspect and elevation were computed for each hillslope, and the topographic layer was combined with land use and vegetation layers to create polygons, which were further aggregated or subdivided to form HRUs. They verified the model by comparing results to a time series of snow-covered area maps and streamflow.

Hendrick *et al.* (1971) used a simple distributed energy balance model to predict snowmelt in the Sleepers River watershed in Vermont. The purpose of the study was to investigate the effects of topographic and forest cover variations on snowmelt rates. The watershed was divided into 96 modeling units, based on slope, aspect, elevation and vegetation cover. They found that spatial diversity in forest cover, elevation and slope-aspect have a large influence on the spatial variation of snowmelt rates, leading to a staggered release of meltwater over the basin. They concluded that highly heterogeneous

basins are less prone to snowmelt flooding events than basins that are homogeneous in terrain and/or forest cover, and that when modeling snowmelt, variations in terrain and vegetation should be included in the model.

Baral and Gupta (1997) used DEM-derived slope and aspect characteristics of a small, Himalayan basin to create 12 slope-aspect classes, described as “landform facets”. Slope was divided into gentle ($<22.5^\circ$), moderate ($22.5^\circ - 45^\circ$) and steep ($>45^\circ$) and aspect was divided into north, south, east and west. Snow-covered pixels were calculated by superimposing SCA images onto the landform facet image. They found that south-facing facets had the most snow covered area and the fastest snow depletion, whereas north-facing facets had the least snow covered area and slowest snow depletion. The west-facing facets had more snow-covered pixels and faster depletion than the east-facing facets. All steep slopes and cliffs exhibited a similar pattern of depletion, but accounted for a very small proportion of total land and snow-covered area.

Becker and Braun (1999) examined the effect of spatial resolution of HRUs using a disaggregation/aggregation scheme to create varying sizes of HRUs in a small basin in northern Germany. They considered nine levels of aggregation, each with a different level of detail based on land use, land cover, slope class, and soil characteristics. At the most detailed resolution, 4540 HRUs were created, and classes were then progressively combined according to hydrologic response until nine aggregation sets were achieved. For each level of aggregation, the Nash-Sutcliffe measure of model efficiency was used to evaluate predicted runoff. They found that model efficiency was improved by segregating modeling units according to the natural mosaic of the land surface, but that the most efficient combinations are not necessarily the ones with the most HRUs.

Cline *et al.* (1998) investigated the effect of increasing spatial and temporal resolutions on modeled distributions of SWE and snowmelt in the Emerald Lake Watershed in the Sierra Nevada, California. They found that although coarsening the spatial resolution from 30 m to 250 and 500 m did not significantly alter the estimation of basin-wide peak SWE, it did result in a loss of explicit information regarding the location and distribution of SWE in the basin. They also found that at a 90 m spatial scale and all temporal resolutions (1 hr, 3 hr and 6 hr meteorological input), mean basin SWE was overestimated by 14-17%. These results suggest that either the particular combination of slopes, aspects, elevations and snow covers at 90 m resolution created a very different distribution of SWE or there exists a spatial scale threshold such as that described by the REA concept of Wood *et al.* (1988).

2.2 SNOW-COVERED AREA DEPLETION CURVES

Through a survey of recent developments in distributed snowmelt modeling, Kirnbauer *et al.* (1994) determined that comparison of model results to snow cover depletion patterns have two important advantages over comparison to streamflow for model verification: 1) SCA depletion patterns have the advantage of spatial and temporal representativeness, and 2) they allow for the spatially distributed assessment of the model. Depletion curves have been used to predict runoff volumes for operational forecasts based on temperature-index-based melt (e.g. Anderson, 1973; Martinec, 1985) and have been used to inform modeled evolution of snow water equivalent in the snowpack (e.g. Dunne and Leopold, 1978; Buttle and McDonnell, 1987; Luce and Tarboton, 2004).

Leaf (1969) estimated change in snow covered area in three small basins within the Fraser Experimental Forest, Colorado, using a time-series of aerial photographs. The photographs were transposed onto base maps of each watershed that had been subdivided into homogeneous areas according to classes of elevation, slope, aspect and vegetation. It was found that within each homogeneous area, conditions of the snowpack were uniform and changed abruptly with respect to other units. The results were expressed with depletion curves relating changes in SCA to “cumulative runoff” and concluded that each study basin has a characteristic functional relationship between changes in SCA and runoff during the melt season. It was also suggested that year-to-year differences may be explained by factors such as initial snowpack water equivalent, antecedent soil moisture conditions and meteorological conditions during snowmelt.

Anderson (1973) concluded that areal snow cover could be empirically related to accumulated runoff by deriving curves directly from observed data or by a mathematical equation relating snow-covered area to cumulative generated runoff. Snow-cover depletion can also be related to temperature or some other index of melt. Empirical SCA curves can be related to either cumulative runoff starting from date of peak SWE, or “future runoff” taken by accumulating runoff from the end of the melt season to peak SWE (USACE, 1953; 1956).

2.3 MODEL APPLICATIONS

2.3.1 FASST

Fast All-Season Soil STrength (FASST) (Frankenstein and Koenig, 2004) is a relatively new model and has little exposure in the literature. FASST is a one-dimensional soil strength and surface friction model designed for use in seasonally snow-covered environments. Holcombe (2004) found that FASST successfully predicted snow depth when compared to observed snow depth at a shallow (<0.5 m), windblown site in Colorado. Frankenstein *et al.* (2007) found that FASST successfully reproduced snow depth predictions at a deep (> 2 m) unforested site and a moderate (~1.5 m) forested site in Colorado. A full description of FASST as it was used in this study is given in Chapter 5, Section 5.1.

2.3.2 SNOWMODEL

SnowModel is a snow evolution modeling system composed of four sub-models (MicroMet, EnBal, SnowTran-3D and SnowPack) that have all been individually developed and tested in a variety of global snow environments. The suite of SnowModel was first presented by Liston and Elder (2006a) who found that SnowModel closely reproduced observed SWE distribution, time evolution, and interannual variability patterns at adjacent forested and clear-cut sites in Colorado and a small (0.38 km²) basin in southwestern Idaho. Liston *et al.* (2007) used SnowModel to simulate realistic snow water equivalent distributions using a 30 m grid resolution over three 30 km by 30 km domains in Colorado, each exhibiting unique topography, vegetation, meteorological and snow-related characteristics. These domains were centered over 25 km x 25 km Meso-

cell study areas (MSAs) included as part of the NASA Cold Land Processes Field Experiment (CLPX) (Cline *et al.*, 2003). Results from simulations of SWE distribution over the Fraser MSA were used as input for model initialization in this study.

MicroMet, the meteorological data assimilation and distribution sub-model within SnowModel, was developed and tested over the Rabbit Ears MSA (Liston and Elder, 2006b). Meteorological data used was from a variety of sources, including nine data points from the National Oceanic and Atmospheric Association's (NOAA) gridded Local Analysis and Prediction System (LAPS) and eight independent meteorological station datasets from a variety of sources. Four simulations were performed using a successive decrease in amount of meteorological input data, with the finest resolution being all available weather data as described above, and the coarsest being data from two meteorological towers. It was found that the model successfully interpolated and distributed irregularly spaced station observations using the Barnes objective analysis scheme over the Rabbit Ears MSA, with the most realistic distribution coming from the finest resolution of input data.

The energy balance model within SnowModel (later termed "EnBal) was developed by Liston (1995) and used to simulate the melt of patchy snow covers over a 10 km horizontal domain. The model was then coupled with a snow accumulation and depletion model (later termed "SnowPack) to simulate lake-ice accumulation and depletion (Liston and Hall, 1995). The coupled energy balance and snow accumulation models were tested against lake-ice observations at Glacier National Park made during the winter of 1992-1993. EnBal was later used to simulate differences in solar radiation

extinction profiles and below-surface ice melt between snow and ice layers on a coastal Antarctic ice sheet (Liston *et al.*, 1999).

SnowTran-3D was developed to simulate three-dimensional snow depth distribution over topographically variable terrain influenced by interactions between snowfall, wind and topography, and tested using snow depth data collected north of the Brooks Range in Alaska over a period of four years (Liston and Sturm, 1998). Liston *et al.* (2006) enhanced the original SnowTran-3D, creating a generalized version (version 2.0) with three major improvements: 1) an improved sub-wind model, 2) a two-layer sub-model describing the threshold friction velocity that must be exceeded to transport snow, and 3) a 3-dimensional drift profile sub-model which forces SnowTran-3D to evolve snow accumulations toward observed profiles. This paper also coupled SnowTran-3D with MicroMet to provide distributed atmospheric data for input into SnowTran-3D.

CHAPTER 3. OBJECTIVES

This study had three main objectives: 1) evaluate the capability of Fast All-Season Soil Strength (FASST) and SnowModel to predict point estimates of snow depth at two subalpine forested sites within the Fraser Experimental Forest; 2) explore the influence of spatial scale and topographic controls on snowmelt in a mid-latitude, high-elevation Rocky Mountain basin within the Fraser Experimental Forest, Colorado, using SnowModel; and 3) compare runoff and snow-covered area depletion output from SnowModel simulations to gauged basin runoff.

The first objective was met by using FASST and SnowModel to predict snow depth and snow water equivalent (SWE) depletion at two sub-alpine forested sites with differing physiographic characteristics within the study area. Snow depth depletion simulations were compared to observations at each site.

The second objective was met by segregating the study area, St. Louis Creek basin (85.2 km²), into hydrologic response units (HRUs) based upon factors most affecting snow cover depletion such as elevation, aspect, slope and vegetation. The HRUs were segmented into five groups of decreasing polygon numbers and average polygon size, with the greatest number of polygons being 3726 and the least being a single polygon representing the basin as a whole. These simulations tested the hypothesis that SnowModel could successfully predict snow cover and snow water equivalent (SWE)

depletion rate and timing for each simulation, with differences between simulations being a result of physiographic differences between polygons, the polygon averaging scheme and/or number of modeling units. These simulations also tested the hypothesis that the most realistic output would likely come from the finest resolution of modeling units. Results were expressed with spatial distributions of SWE and basin average SWE and snow-covered area depletion curves.

The final objective was met by comparing SnowModel runoff output to reconstructed St. Louis Creek discharge and creating depletion curves that compared predicted snow-covered area to reconstructed discharge.

CHAPTER 4. STUDY AREA

The study area is within the boundaries of one of the NASA Cold Land Processes Field Experiment (CLPX) 25 km x 25 km Meso-cell Study Areas (MSAs) in Colorado (Cline *et al.*, 2003). Each MSA is broadly characterized by topography, vegetation and climate chosen to represent a significant portion of the major global snow cover environments.

The study basin, St. Louis Creek (85.2 km²), lies within the Fraser MSA (Figure 4.1). The Fraser MSA is an area of high relief with dense predominantly coniferous subalpine forests and alpine tundra above treeline. Moderate to deep snowpacks are typical, increasing with elevation (Cline *et al.*, 2003). St. Louis Creek basin has a predominantly north-northeasterly aspect with an average slope of 19°, ranging in elevation from 2743 – 3904 m a.s.l. (USGS, 2006). The land cover is 74% coniferous forest with 23% of the basin above treeline (~3350 m) (USGS, 2001). Discharge data from two smaller gauged basins within St. Louis Creek, East St. Louis Creek (8.03 km²) and Fool Creek (2.89 km²) were also included in this study.

Soils on forested slopes are largely derived from granite and schist. These soils are poorly developed, contain little silt and clay, are highly permeable and have high water storage capacity during snowmelt (Alexander *et al.*, 1985). Soils on the valley floor tend to be a mix of glacial till, glacial outwash and recent valley fill.

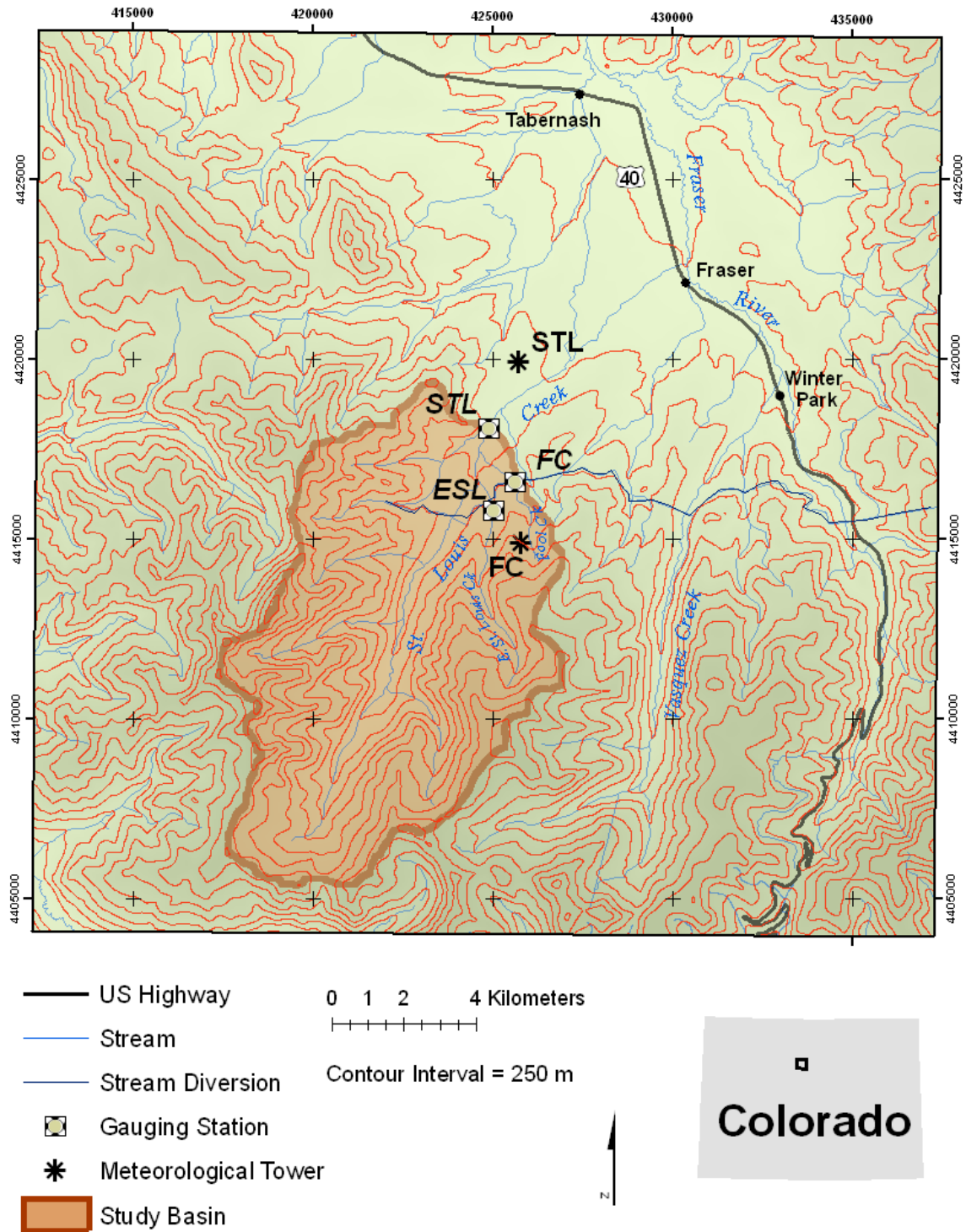


Figure 4.1. Fraser Meso-cell study area (MSA). STL=St. Louis Creek, ESL=East St. Louis Creek, FC=Fool Creek.

There are two meteorological towers within the Fraser MSA that were used in this study for point estimations of snowmelt. St. Louis Creek (STL) meteorological tower is at 2727 m a.s.l. in a flat clearing and Fool Creek (FC) meteorological tower is at 3100 m a.s.l. on a forested 20° slope with a southerly aspect. Precipitation gauges are located a short distance from the meteorological towers: Lower Fool Creek gauge is approximately 500 m northeast of the Fool Creek meteorological tower, and the Fraser Headquarters gauge is located approximately 2700 m southwest and 36 m higher in elevation than the St. Louis Creek tower.

CHAPTER 5. MODELS

5.1 FASST

Fast All-season Soil Strength (FASST) is a one-dimensional state of the ground model originally designed to predict soil strength and surface friction for vehicle mobility and personnel movement (Frankenstein and Koenig, 2004). FASST performs two fundamental calculations: an energy and water balance quantifying both the flow of heat and moisture within the soil, and the exchange of heat and moisture at all interfaces (ground/air or ground/snow and snow/air). FASST uses up to nine modules, including a Snow Accretion-Depletion Module (Module 7), which is the module most pertinent to this study. Module 7 predicts variables such as snow depth, snow water equivalent (SWE) and amount of water available from snowmelt. Information about modules not pertinent to this study may be obtained from the FASST technical documentation (Frankenstein and Koenig, 2004). Refer to Figure 5.1 for a flow chart of FASST as used in this study.

Module 7 is a physically-based approach to modeling snowmelt, where the melt is driven by an energy balance at the snow surface and the physics of meltwater flow through the snowpack are considered. At temperatures below freezing, incoming precipitation is converted to a snowfall amount and added to the existing snowpack. Flow of meltwater through the snowpack is governed by gravity, rather than capillarity and is based on a simplified form of Darcy's equation:

$$U = \frac{p_w k_w g}{\eta_w} \quad (5.1)$$

where U (cm/s) is the volume flux of water, p_w is the density of water (1000 kg/m³), k_w (cm²) is the relative permeability to water, g is the gravitational constant (981 cm/s), and η_w is the viscosity of water (g/cm·s). Modifications of Equation 5.1 are made to account for layering in the snowpack, and the solution to the flow equations at any given timestep are also a function of boundary conditions and meteorological input at that particular timestep. Water flow through the pack is modeled as a series of flux waves that can continually overtake each other on the way to the bottom of the snowpack.

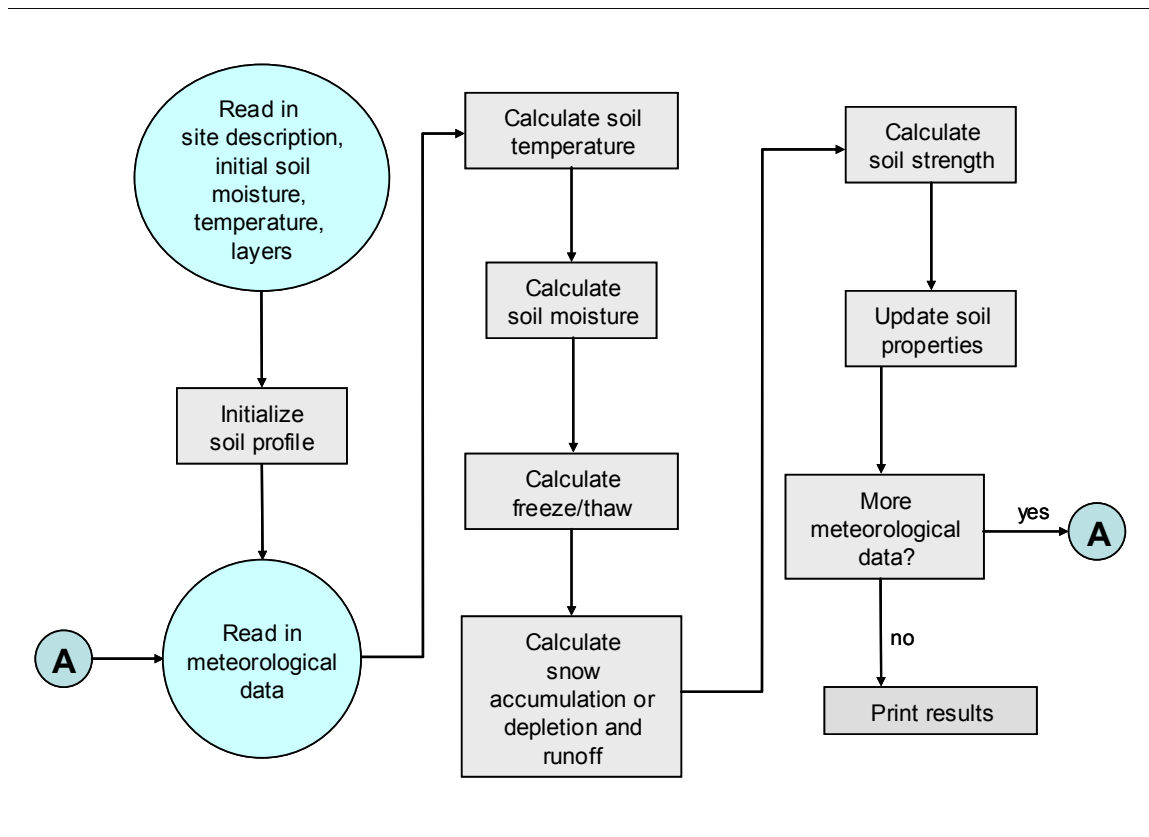


Figure 5.1 Flow chart of FASST model processes as used in this study.

Grain size is currently used only to calculate the permeability of snow, where permeability is a function of both grain size and snow density. The rate of densification of the snowpack is essential for calculating the depth of the snowpack at any given point in time. Densification is based on the work of Jordan (1991) and Anderson (1973), who establish densification rate as a function of snow metamorphism and overburden load pressure. The equations used are as follows:

$$\left. \frac{1}{D_s} \frac{\partial D_s}{\partial t} \right|_{\text{metamorphism}} = -2.778 \times 10^{-6} c_1 c_2 \exp[-0.04T] \quad (5.2)$$

where D_s is the depth of snow (cm), t is time (s), T is temperature ($^{\circ}\text{C}$), and

$$c_1 = 1 \quad \rho_i \leq 0.12 \quad (5.3)$$

$$c_1 = \exp[-46(\rho_i - 0.15)] \quad \rho_i \geq 0.12 \quad (5.4)$$

where ρ_i (g/cm^3) is the density of water in the frozen state within the snowpack and

$$c_2 = 1 + f_i \quad (5.5)$$

where f_i is the fraction of the snowpack that is wet. Densification due to overburden is calculated as follows:

$$\left| \frac{1}{D_s} \frac{\partial D_s}{\partial t} \right|_{\text{overburden}} = -\frac{\bar{P}_s}{\eta_c} \quad (5.6)$$

where \bar{P}_s (g cm/s^2) is the average load pressure within the snowpack and η_c is a viscosity coefficient ($\eta_c = 3.3$).

To estimate snowmelt, FASST uses a full surface energy balance. The heat input at the top of the snowpack I_{top} (W/m^2) is calculated using

$$I_{top} = I_s \downarrow (1 - \alpha_s) + I_{ir} \downarrow - I_{ir} \uparrow + H + L + I_{conv} \quad (5.7)$$

where $I_s \downarrow$ (W/m^2) is net solar radiation at the surface, α_s is the snow surface albedo, $I_{ir} \downarrow$ (W/m^2) is incoming longwave radiation, $I_{ir} \uparrow$ (W/m^2) is outgoing longwave radiation, H (W/m^2) is the sensible heat flux, L (W/m^2) is the latent heat flux and I_{conv} (W/m^2) is the convective heat flux. Melting can occur both at the surface and at the base of the snowpack if the ground temperature calculated at that timestep is above freezing. Surface albedo of the snowpack is calculated using three different methods at each timestep: 1) upwelling shortwave radiation divided by downwelling short wave radiation ($\alpha_s = S_{up}/S_{down}$); 2) using the method of Douville *et al.* (1995) (α_{sD}); and 3) using the surface temperature dependent method of Roesch (2000) where maximum albedo is set to 0.8 and minimum is set to 0.5 (α_{sR}). The final albedo used at each timestep is the minimum of (S_{up}/S_{down}) or ($\max(\alpha_{sD}, \alpha_{sR})$).

Required inputs for the snow accretion/depletion module are air temperature ($^{\circ}\text{C}$), wind speed (m/s) and precipitation amount (cm). Net solar radiation (W/m^2), net longwave radiation (W/m^2) and precipitation type can be input or estimated by the model.

If available, snow properties such as initial snow depth (cm), snow water equivalent (cm), initial water saturation, effective porosity (default 0.228), and snow surface temperature (°C) may be input, otherwise the model will compute those parameters. Output from Module 7 is snow depth (cm), amount of melt that has been released from the snowpack (cm) and new snow density (g/cm³).

5.2 SNOWMODEL

SnowModel is a spatially-distributed snow accumulation and depletion modeling system designed for application in a variety of landscapes where snow occurs (Liston and Elder, 2006a). SnowModel is an aggregation of four sub-models: MicroMet, a quasi-physically based model which assimilates and interpolates meteorological data from a variety of sources (Liston and Elder, 2006b); EnBal, a surface energy exchange model (Liston, 1995; Liston *et al.*, 1999); SnowTran-3D, a three-dimensional blowing snow model which takes terrain and vegetation into account (Liston and Sturm, 1998; Liston *et al.*, 2006); and SnowPack, a simple one-layer snowpack evolution model (Liston and Hall, 1995). Modifications to each of the above sub-models, which were originally created to run in non-forested environments, were made to simulate processes in forested areas. SnowModel can run on increments of 10 minutes to 1 day and spatial grid scales of 5- to 200 m and also on significantly larger grid increments if the inherent loss in explicit information regarding snow distribution is acceptable. At a minimum, SnowModel requires a time series of air temperature, relative humidity, precipitation and wind speed and direction along with spatially-distributed fields of topography and vegetation type. Refer to Figure 5.2 for a flow chart of SnowModel as used in this study.

Descriptions of MicroMet, EnBal and SnowPack are given here. SnowTran-3D was not used in this study for a number of reasons, including the assumption that an ablating snowpack is less likely to be modified by wind. Refer to Liston and Elder (2006a) for documentation of SnowTran-3D within SnowModel.

For the purpose of this study, MicroMet was modified to output average distributed meteorological forcings over each polygon. The number of grid cells in each polygon was calculated and meteorological data for each timestep at each grid cell within that polygon were summed and averaged to produce a set of meteorological forcings that act as a meteorological “tower” in the middle of each polygon. This method also accounts for slope and aspect within each polygon. However, this form of averaging does not produce correct results for wind direction over the 0°/360° line, but wind direction is only required to run SnowTran 3-D, which was not used in this study.

Polygon meteorological distributions were first created by MicroMet and then used as input into EnBal and SnowPack. This method allowed for the simulation of each HRU as an independent modeling unit.

5.2.1 MICROMET

MicroMet is a quasi-physically based, intermediate complexity model designed to produce high-resolution (i.e. 30 m to 1 km) meteorological data distributions required to run spatially distributed terrestrial models over a variety of landscapes (Liston and Elder, 2006b). MicroMet includes a three-part preprocessor that analyzes and corrects deficiencies in meteorological station data or model grid point data.

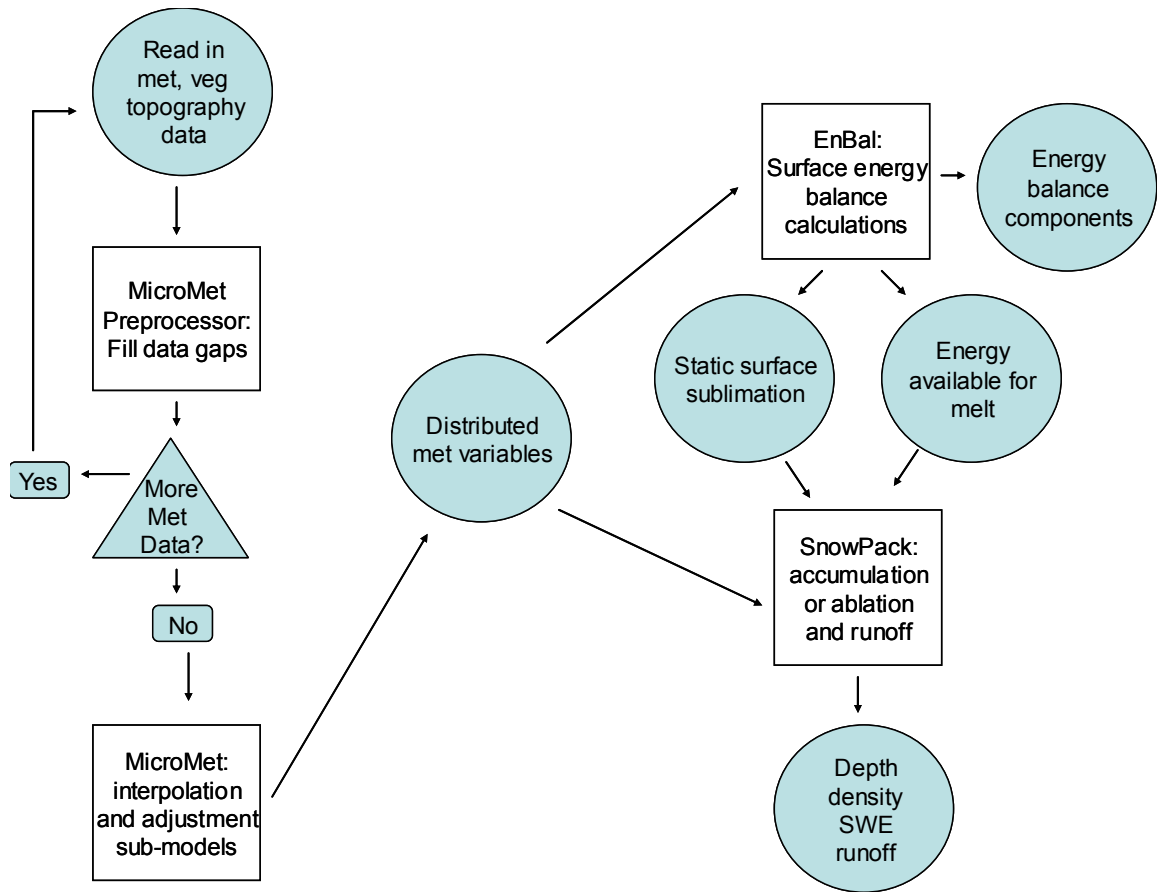


Figure 5.2 SnowModel flow chart for processes used in this study.

Required meteorological inputs for MicroMet at each time step are air temperature, relative humidity, wind speed, wind direction and precipitation. MicroMet can either assimilate observations of incoming solar and longwave radiation and surface pressure to create distributions or it can generate them from its sub-models.

The MicroMet preprocessor performs three functions: filling variables for missing dates/times with an “undefined” value (i.e. -9999), performing a series of QA/QC data tests following Meek and Hatfield (1994), and filling in missing time series data with calculated values. Data is filled in a variety of ways depending on the length of the

missing data segment with the assumption that air temperature, wind speed and direction, relative humidity and precipitation are all subject to diurnal cycles.

The MicroMet model uses known relationships between meteorological variables and the landscape (primarily topography) to distribute those variables over the domain. MicroMet first spatially interpolates all available station data over the domain using a Barnes objective analysis scheme and then physical sub-models are applied to each meteorological variable to improve estimates at a given point in time and space. The objective analysis is the process of interpolating data from irregularly spaced stations to a regular grid, and the Barnes scheme applies a Gaussian distance-dependent weighting function in which the weight that a station contributes to the overall value of the estimated grid point decreases with increasing distance from this point. The Barnes technique employs the method of successive corrections, applying two passes through the station data to reduce random errors.

After interpolation, physical sub-models are applied to each meteorological variable to further improve grid point estimates based on known relationships between each variable and the surrounding landscape. Sub-models for wind speed and incoming solar and longwave radiation assume top-of-canopy conditions. A brief description of each sub-model is given here, after Liston and Elder (2006a; 2006b). For complete documentation of each sub-model, refer to Liston and Elder (2006b).

1. **Air temperature** is adjusted based on the known relationship between air temperature and elevation. Station air temperatures are adjusted to a common level by applying default lapse rates that vary seasonally or are calculated based on adjacent station data. This study uses the default lapse rates. The reference-level station

temperatures are then interpolated to the model grid using the aforementioned Barnes interpolation scheme. The available topography data and lapse rates are then applied to adjust the reference-level temperatures to the elevations provided by the topography grid.

2. **Relative humidity**, which is largely non-linear with respect to elevation, is converted to dewpoint temperature, which varies relatively linearly with elevation. Once converted, data are applied to a reference level using a dewpoint temperature lapse rate which varies monthly. The reference-level station dewpoints are then interpolated to the model grid using the Barnes interpolation scheme. The dewpoint lapse rate is applied to the reference level grid to adjust each gridpoint to the topography grid. The gridded dewpoint values are then converted back to relative humidity.

3. **Wind speed and direction** values are inherently problematic due to interpolating over the $0^{\circ}/360^{\circ}$ line. Therefore, wind speed and direction values are converted to zonal (u) and meridional (v) components, which are functions of wind speed and direction at each timestep. The u and v components are interpolated independently using the Barnes objective analysis scheme. The values are then converted back to wind speed and direction. The gridded wind speed and direction values are modified using a simple, topographically driven wind model following Liston and Sturm (1998) that adjusts speed and direction according to topographic slope and curvature relationships. The final speeds are adjusted according to a diverting factor, which is added to the wind direction to yield the terrain-modified wind direction.

4. **Incoming solar radiation** is adjusted using model time to determine the influence of time of day, cloud cover, direct and diffuse solar radiation and terrain. Cloud cover is estimated by first taking gridded air temperature and dewpoint temperature (as

described above) and the associated lapse rates to determine temperature and dewpoint at the 700 mb level. Using the temperature and dewpoint values, relative humidity can be calculated at the 700 mb level, and the relative humidity distribution is used to define cloud cover fraction. If available, incoming solar radiation observations can be assimilated into this calculation using MicroMet.

5. **Incoming longwave radiation** is adjusted while taking into account cloud cover and elevation-related variations, which is particularly valid in mountainous areas. If available, incoming longwave radiation observations can be assimilated using MicroMet.

6. **Surface pressure** can either be provided or calculated using a time-dependent surface pressure distribution.

7. **Precipitation** is initially interpolated to the model grid using the Barnes objective analysis scheme. The station elevations are also interpolated to the model grid to generate a topographic reference surface. The interpolated station elevations are used as a reference surface rather than sea level since the precipitation adjustment factor is a non-linear function of elevation. The modeled precipitation rate equals the product of the interpolated station precipitation and a monthly-varying empirical topographic adjustment factor. Therefore, a non-linear precipitation increase (decrease) results from increasing (decreasing) elevation from the topographic reference surface.

5.2.2 ENBAL

EnBal is a simple surface energy balance model (Liston, 1995; Liston *et al.*, 1999) that simulates surface temperatures and energy and moisture fluxes in response to near-

surface meteorological forcings provided by MicroMet. Surface sensible and latent heat flux and snowmelt are made using an energy balance model of the form:

$$(1 - \alpha)Q_{si} + Q_{li} + Q_{le} + Q_h + Q_e + Q_c = Q_m \quad (5.8)$$

where α is snow surface albedo, Q_{si} (W/m^2) is incoming solar radiation striking Earth's surface (accounting for terrain), Q_{li} (W/m^2) is incoming longwave radiation, Q_{le} (W/m^2) is emitted longwave radiation, Q_h (W/m^2) is turbulent exchange of sensible heat, Q_e (W/m^2) is the turbulent exchange of latent heat, Q_c (W/m^2) is conductive energy transport and Q_m (W/m^2) is the energy flux available for melt (Liston and Elder, 2006a).

SnowModel defines different albedos for snow below forest canopies, snow in forest clearings, and glacier ice surfaces. A complete description of the model solution and details of each term in Equation (5.8) can be found in Liston (1995), Liston and Hall (1995) and Liston *et al.* (1999). Equation (5.8) is solved by applying equations to each term that have been set to leave surface temperature as the only unknown. The melt energy is then defined to be zero and Equation (5.8) is solved iteratively for surface temperature. If surface temperatures are greater than 0°C in the presence of snow, it is assumed that there is energy available for melt and this energy is computed by fixing the surface temperature at 0°C and solving for Q_m .

5.2.3 SNOWPACK

SnowPack is a single layer snow accumulation and depletion model (Liston and Hall, 1995). SnowPack defines changes in the snowpack in response to the melt fluxes

and precipitation input given by MicroMet. Compaction-based snow density evolution closely follows that of Anderson (1976) (*in* Liston and Hall, 1995) where density changes with time in response to snow temperature and weight of overlying snow. Additionally, snow melting alters snow density by decreasing snow depth and redistributing meltwater through the snowpack until a maximum snow density is reached. Any excess meltwater is assumed to reach the ground at the base of the snowpack and is available for melt runoff. New snow density is calculated after Anderson (1976) (*in* Liston and Hall, 1995) and added to the existing snowpack accordingly. Non-blowing snow sublimation is calculated in EnBal and used to adjust snowpack depth (Liston and Elder, 2006a).

6. DATA AND METHODS

6.1 POINT SIMULATIONS

6.1.1 METEOROLOGICAL INPUTS

Meteorological data (except precipitation) used for point simulations (Table 6.1) were collected from March-June, 2003 at Fool Creek and St. Louis Creek meteorological towers. These towers were installed at part of the NASA (CLPX) and include instrumentation to measure the following: air temperature, relative humidity, wind speed and direction, snow depth, and snow surface temperature measured at 3 m above ground within the Fraser MSA. Soil temperature was measured at 0, 0.05, 0.20, and 0.50 m below ground surface. Incoming and outgoing shortwave radiation and upwelling and downwelling longwave radiation were measured at 10 m above ground level, or approximately above the canopy. Snow depth, wind direction and soil temperature were recorded as single sample measurements at the start of each 10-minute time period. All other observations made at 30-second intervals were averaged and recorded at 10-minute intervals. Observations were recorded using Campbell Scientific CR10X dataloggers.

The data were previously processed to a Level 1 standard, meaning that raw data downloaded from dataloggers were filtered once manually to recognize instrument, wiring or programming problems and computationally filtered a second time to remove blank values or faulty values that fell outside the accuracy range of each instrument (Elder and Goodbody, 2004).

Table 6.1. Meteorological parameters used in this study and instrumentation, after *Elder and Goodbody (2006)*. All instruments, with the exception of precipitation gauges, are located on the Fool Creek and St. Louis Creek meteorological towers. Also included is which model uses which meteorological forcing data.

Variable	Instrumentation	Used in which model(s)
Air Temperature (°C)	Vaisala HMP45C Temperature and Relative Humidity Probe	FASST and SnowModel
Relative Humidity (%)	Vaisala HMP45C Temperature and Relative Humidity Probe	FASST and SnowModel
Air pressure (mb)	Vaisala PTB101B Ressure Transmitter	FASST
Wind Speed (m/s)	R. M. Young 05103 Wind Monitor	FASST and SnowModel
Wind Direction (°)	R. M. Young 05103 Wind Monitor	SnowModel
Snow Depth (m)	Judd Ultrasonic Depth Sensor	FASST and SnowModel (initial snow depth only)
Average Hydraprobe (Soil) Temperature (°C)	Stevens Vitel Hydro Soil Moisture Probe	FASST
Incoming and Outgoing Shortwave Radiation (W/m ²)	Kipp and Zonen CNR1 Net Radiometer	FASST
Upwelling and Downwelling Longwave Radiation (W/m ²)	Kipp and Zonen CNR1 Net Radiometer	FASST
Precipitation near Fraser Headquarters	Dual traverse 12-inch capacity Belfort precipitation gauge	FASST and SnowModel
Precipitation near Fool Creek meteorological tower	National Weather Service standard 10-inch precipitation gauge	FASST and SnowModel

Blank and missing values were filled with a default value of 8999. Original 10 minute interval data were averaged or summed (depending on the nature of the parameter) to produce an hourly time series for use in FASST and SnowModel.

Since precipitation gauge locations were not coincident with meteorological tower sites, incoming SWE was initially estimated from snow depth sensor data by assuming a new snow density of 100 kg/m^3 for simplicity, after Thyer *et al.* (2004). FASST model results using this technique were compared to results using 2003 precipitation data from a standard National Weather Service 10-inch precipitation gauge, located 500 m downhill from the Fool Creek meteorological tower. The results suggested that data from the nearby precipitation gauge provide similar estimates of incoming precipitation and eliminates the noise inherent in depth sensor measurements (i.e. Brazanec, 2005). Additionally, it was found that noise from sensor data overwhelmed SnowModel with excessive “apparent” incoming precipitation. Although gauge undercatch is certainly a source of error in precipitation measurements (e.g. Goodison, 1978; Yang *et al.*, 2000; Fassnacht, 2004), it was decided that using gauge precipitation data was more suitable than attempting to determine and delete all false trace events from snow depth sensor data.

Hourly precipitation data at St. Louis Creek were derived by manually digitizing strip charts from a precipitation gauge near Fraser Headquarters (Table 6.1), located approximately 2700 m southwest of the St. Louis Creek meteorological tower, and 36 m higher in elevation. All charts were visually scanned for errors, and hourly precipitation data were totaled for the week and compared to the weekly bucket weight measurements.

Discrepancies in the hourly data were adjusted to match the weekly bucket weights.

Precipitation data from the Fool Creek gauge was digitized using the same methodology.

6.1.2 SOIL

Soil data for input into FASST were derived from Retzer's (1962) Fraser soil survey. One of the available default USCS (Unified Soil Classification System) soil types within FASST was chosen for each site by matching soil characteristics from the survey to the description of the USCS soil types. The Fool Creek soil was classified as a silty-gravel, gravel-sand-silt mixture (USCS soil type "GM"). The St. Louis Creek soil was classified as a combination of a silty sand, sand-silt mixture and a clayey-sand, sand-clay mixture (USCS soil type SMSC). The only soil parameter measured in the CLPX survey that was used in FASST was bulk density. The value for bulk density at each site was averaged from measurements taken at seventeen locations within each ISA. Average bulk density across the Fool Creek ISA was 1.1 g/cm^3 and across the St. Louis Creek ISA was 1.02 g/cm^3 (Elder and Goodbody, 2004). The remaining soil parameters were set to default values within FASST according to the USCS soil type at each site. A list of soil parameters used by FASST is summarized in Table 6.2.

6.1.3 FASST INITIALIZATION

FASST was initialized using soil and snowpack physical data collected near the time of peak accumulation and forced by hourly meteorological data (Table 6.1) until complete snowpack ablation occurred. The Fool Creek site was simulated for the period

of 26 March, 2003 through 4 June, 2003. The St. Louis Creek site was simulated for the period of 23 March, 2003 through 21 May, 2003.

Steady state parameters input into FASST were site location, slope, aspect and elevation. Initial snow depth was obtained from the depth sensor and soil temperatures at 0.05, 0.10, 0.20 and 0.50 m below ground surface were used to initialize the model. Initial snow surface albedo was set to 0.8.

Table 6.2. Soil parameters used by FASST, after *Frankenstein and Koenig (2004)*. Any parameters not provided by the user are set as default values within FASST.

Parameter	Units (if applicable)
Bulk density of dry material	g/cm ³
Intrinsic density of dry material	g/cm ³
Volume fraction of solids	-
Porosity	-
Void ratio	-
Albedo	-
Emissivity	-
Quartz content	-
Organic fraction	-
Thermal conductivity of dry material	W/m*K
Specific heat of dry material	J/kg*K
Saturated hydraulic conductivity	cm/s
Residual water content	vol/vol
Maximum water content	vol/vol
van Genuchten bubbling pressure head	cm
van Genuchten exponent	-
Rating cone index/moisture content coefficient 1	-
Rating cone index/moisture content coefficient 2	-

6.1.4 SNOWMODEL INITIALIZATION

The same time periods were used for simulations of SnowModel as were used for FASST. The steady state parameters input into SnowModel were site elevation and location. SnowModel was initialized using snow depth from the depth sensor. Meteorological parameters used in SnowModel are summarized in Table 6.1.

A melting snow albedo of 0.50 was used at Fool Creek and a melting snow albedo of 0.60 was used at St. Louis Creek. A range of realistic albedos were chosen based on appropriate values from the literature (e.g. Dunne and Leopold, 1978; Male and Gray, 1981; Pomeroy and Dion, 1996; Hardy *et al.*, 1997; Link and Marks, 1999; Melloh *et al.*, 2002) and the final albedo value at each site was chosen based on which value produced simulated snow depth most resembling observed snow depth. Both sites were located in small clearings surrounded by forests, so they were modeled as clearings even though there may be influence from surrounding trees such as increased incoming longwave radiation to the snowpack.

6.2 POLYGON SIMULATIONS

6.2.1 TERRAIN SEGMENTATION AND AGGREGATION

Hydrologic Response Unit (HRU) aggregation was based on common factors affecting snowmelt at various spatial scales such as slope, aspect, elevation and vegetation type. Basin segmentation was based on the work of Leavesley and Stannard (1990) and Hendrick (1971) although greater computing power and advanced software (ArcGIS 9.x) allowed for terrain segmentation at very high spatial resolutions, i.e. the smallest HRUs were 30 m grid cells (900 m²).

In mountainous regions, snowmelt is dominated by net radiation rather than turbulent transfer, as in lowland areas (Kirnbauer *et al.*, 1994). At high elevations, cool air temperatures results in less transfer of sensible heat from the air to the snowpack than at lower elevations of similar latitude. Therefore, factors most affecting net radiation such as elevation, aspect, slope and vegetation cover were the focus of basin segmentation in

this project. The integrated effect of these factors determine the rate of depletion in a basin, and basins with the most diversity in terrain will display the longest period of snow depletion (Hendrick *et al.*, 1971).

6.2.2 TOPOGRAPHIC AND LAND COVER DATA

The 30 m horizontal resolution topographic Digital Elevation Model (DEM) and vegetation data arrays used in Liston *et al.* (2007) were used in this study. These datasets were 30 x 30 km blocks centered over the 25 x 25 km Fraser MSA to ensure complete coverage of the MSA. The DEM used by Liston *et al.* (2007) was from the United States Geological Survey (USGS) National Elevation Dataset (2006) and the vegetation data array was from the USGS National Land Cover Dataset (NLCD) (2001). The NLCD vegetation codes were modified to reflect vegetation codes used in SnowModel, i.e. the NLCD number representing “coniferous forest” is 42, and the number representing “coniferous forest” in SnowModel is 1.

The St. Louis Creek basin was delineated using the USGS GIS Weasel (Viger *et al.*, Undated), which required DEM and basin outlet data. The St. Louis Creek gauging station location was obtained from the USGS online stream database (2006). For ease of processing, the area contained inside the boundary of the basin was isolated (“clipped”) from the 30 km DEM and vegetation array before polygon creation.

6.2.3 SLOPE, ASPECT AND ELEVATION

The incidence of solar radiation on a surface is largely a function of slope and aspect (and time of year, which is accounted for in MicroMet) and south-facing slopes

receive more radiation than north-facing slopes (Male and Gray, 1981). Some steep north-facing areas in mountain basins may not receive direct radiation for one or two months in the winter, while adjacent slopes may receive direct radiation on a regular basis (Elder *et al.*, 1991). Therefore, each basin was segmented into varying classes defining differences in slope and aspect.

The slope surface was created in ArcGIS using a tool that calculates the slope between adjacent grid cells using the elevation of each grid cell in the DEM. Slope was converted to integer values to allow for processing into polygons. The distribution of slope St. Louis Creek Basin is approximately normal with a slight right skew (Figure 6.1). Slope was divided into four groups (A-D) and basin average (E) and are summarized in Table 6.3.

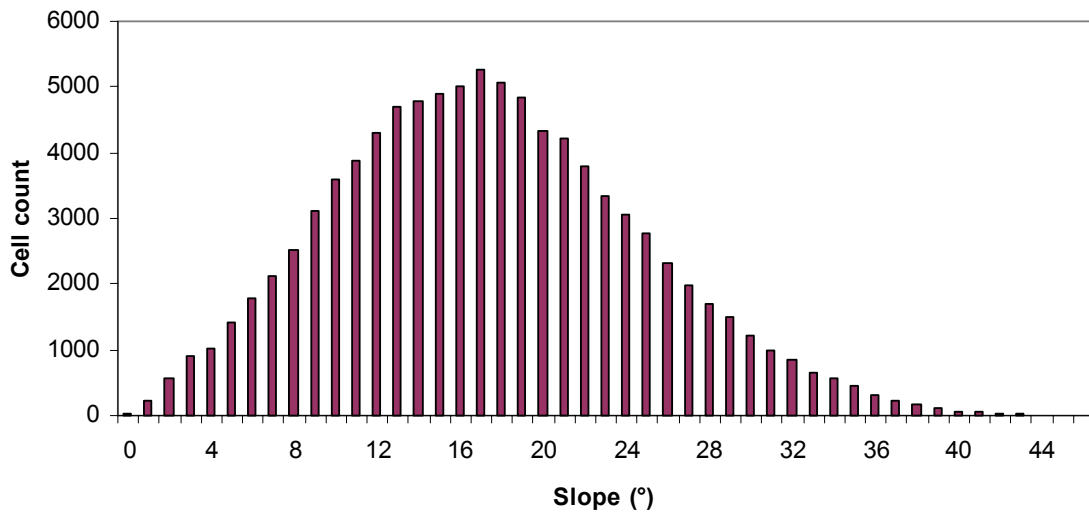


Figure 6.1. Distribution of integer-value slope in St. Louis Creek basin calculated from the 30 m resolution Digital Elevation Model.

Every cell within a given group was assigned the value of the approximate midpoint of each group. For example, the finest resolution of slope (A) was 10-degree increments, i.e. 0°-9°, 10°-19°, etc. and the value assigned to all cells with an original slope between 0° and 9° was 5°, etc. The first coarsening up of resolution (B) was based on the distribution of slope in the basin and slope was divided into “gentle” (0°-12°, value of 6°), “moderate” (12°-22°, value of 17°) and “steep” (22°-46°, value of 34°) after Baral and Gupta (1997). Group C was divided into “shallow” (0°-17°, value of 9°) and “steep” (18°-48°, value of 31°). The last grouping of slope (D) is the same as the previous category, but with “island” cells removed from each layer of slope, aspect, elevation and vegetation. “Islands” were defined as small groups of cells with areas of less than 5 grid cells, or 4500 m². Removing islands serves to increase average polygon size by eliminating high numbers of very small cells. However, once all surfaces were combined (slope, elevation, aspect), some grid cells smaller than 4500 m² were created at intersections of the layers.

Table 6.3. Aggregation groupings for SnowModel simulations, A-E. Simulation D datasets were modified to remove to remove islands of < 5 cells from simulation C datasets. Basin-average slope and aspect are not used as inputs into SnowModel.

	1. Aspect	2. Slope (°)	3. Elevation	4. Vegetation	5. Number of polygons
A. Fine	N/NE/E/SE/S SW/W/NW	5/15/25/35/45	100 m intervals	Original 30 m grid	3726
B. Moderate	N/S/E/W	6/17/34	400 m intervals	“Water” and “bare” lumped with meadow	2395
C. Coarse	N/S	9/31	Treeline	Forested/unforested	579
D. Islands Removed	N/S	9/31	Treeline	Forested/unforested	181
E. Basin	n/a	n/a	3274 m a.s.l.	Coniferous	1

Aspect was divided into four groups (A-D) and basin average (E) based on the cardinal directions and the fact that south-facing slopes receive the most incident shortwave radiation and north-facing slopes receive the least (Table 6.3). The distribution of aspect over the basin is given in Figure 6.2. In each group, the aspect value assigned was the midpoint, in degrees from north, of the group. The finest resolution, group A, was divided into 8 categories: north (347.5° - 22.5° , value 0°), northeast (22.5° - 67.5° , value 45°), east (67.5° - 112.5° , value 90°) etc. Group B was divided into north, south, east and west and group C was divided into north and south. Group D was the same as C, but with islands of 5 or less cells removed.

Slope and aspect were only used in the creation of HRUs and not for direct input into SnowModel. Although SnowModel only uses elevation as a parameter input, slope and aspect were accounted for in the topographic adjustments that were done in MicroMet prior to the averaging of predicted meteorological data for each polygon. Therefore, average basin slope and aspect were not calculated for input into SnowModel.

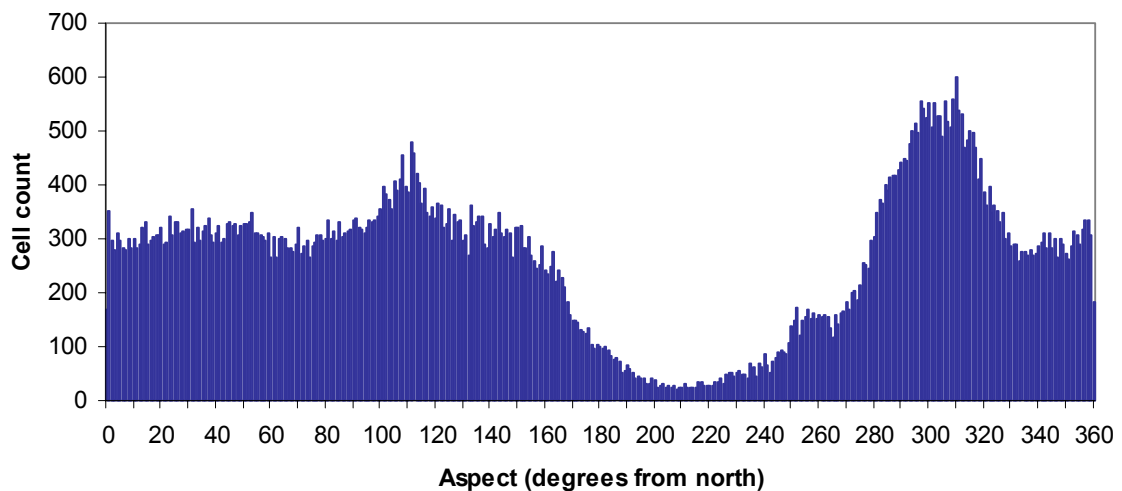


Figure 6.2. Distribution of integer-value aspect in St. Louis Creek basin calculated from the 30 m resolution Digital Elevation Model (DEM).

Longwave radiation and turbulent transfer of sensible heat is affected by air temperature, which is a function of elevation (Dunne and Leopold, 1978). Temperature decrease with elevation is related to the atmospheric lapse rate (Kirnbauer *et al.*, 1994), especially in heterogeneous terrain. Elevation groups were created to simulate temperature change with elevation and to account for basin characteristics such as the presence of a distinct treeline. Elevation groups are listed in Table 6.3 and the distribution of grid cell elevation over the St. Louis Creek basin is shown in Figure 6.3. Group A was divided into 100 m elevation intervals, with the value of each group being the midpoint of the interval, as with slope and aspect. Group B was divided into 400 m intervals and group C was divided into “below treeline” (value 3000 m) and “above treeline” (value 3500 m). Treeline occurs at approximately 3350 m a.s.l. Group D was the same as group C, but with islands of less than 5 cells removed. The basin average elevation was 3274 m a.s.l.

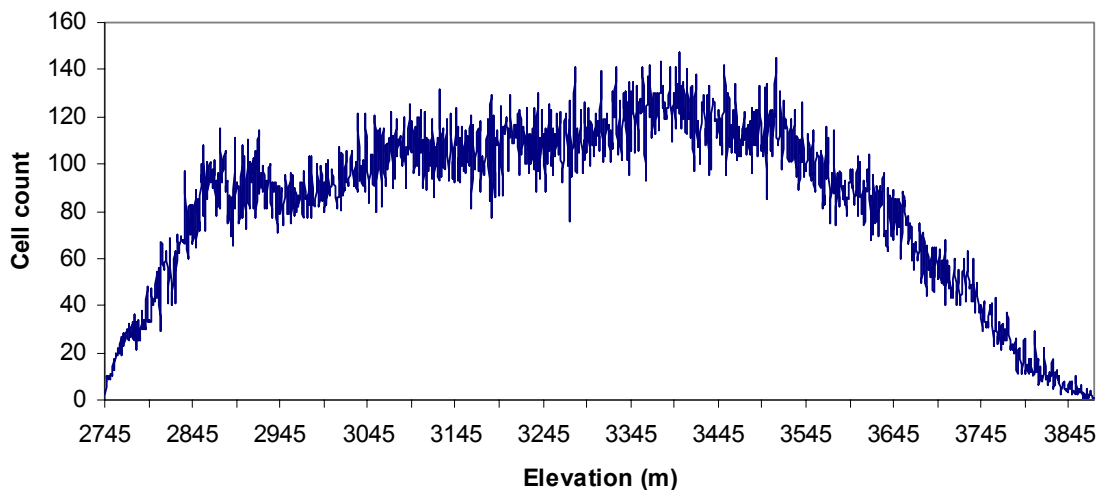


Figure 6.3. Distribution of integer-value elevation in St. Louis Creek basin calculated from the 30 m resolution Digital Elevation Model (DEM).

6.2.4 VEGETATION

A forest canopy above snow acts to reduce incoming shortwave radiation and can increase incoming longwave radiation significantly (Male and Granger, 1981). However, reduced wind speed over the snow in forested areas, resulting in lower turbulent fluxes of sensible and latent heat, can outweigh increased longwave radiative fluxes from the canopy. In turn, it can be expected that melt rates will be lower in areas with greater canopy density (Metcalf and Buttle, 1995). Metcalf and Buttle (1995) found in their study of ablation in forested versus non-forested sites in central Manitoba that open sites at similar elevations ablated much faster than forested sites. However, forested basins with high relief melt at lower elevations with higher temperatures prior to melting out in open areas at higher elevations (i.e. above treeline).

The distribution of vegetation in St. Louis Creek basin is shown in Figure 6.4. The finest resolution of three combinations was the original 30 m grid, with no aggregations. The second combination lumped “water” and “bare” into the “subalpine meadow” category because both snow-covered bare areas and ice or snow-covered ice are likely to have energy budget components similar to snow-covered subalpine meadow areas, as opposed to forested areas. The third classification lumped areas into “forested” and “non-forested” (Table 6.3).

Table 6.4 lists the statistics for each polygon group, including mean, median, and standard deviation of polygon sizes. Figure 6.5 shows the final distributions of polygons in St. Louis Creek. Figure 6.6 shows the distribution of polygon sizes relative to the number of polygons. Although all simulations (A-D) have some very large polygons, the

finer resolution simulations (A and B) have a higher proportion of small polygons relative to the coarser resolution simulations (C and D).

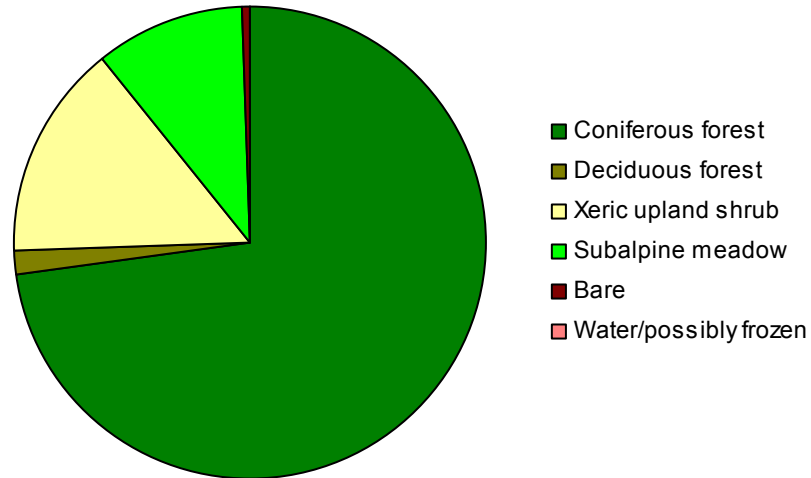


Figure 6.4. Distribution of vegetation cover in St. Louis Creek basin calculated from the 30 m resolution vegetation surface from Liston *et al.* (2006).

Table 6.4. Mean, median and standard deviation of each polygon grouping, simulations A-D.

	Mean polygon area (m ²)	Median polygon area (m ²)	Standard Deviation (m ²)
A (n=3726)	22897	1800	97402
B (n=2795)	35622	1800	297913
C (n=579)	147347	1800	1358401
D (n=181)	471346	9000	2167774

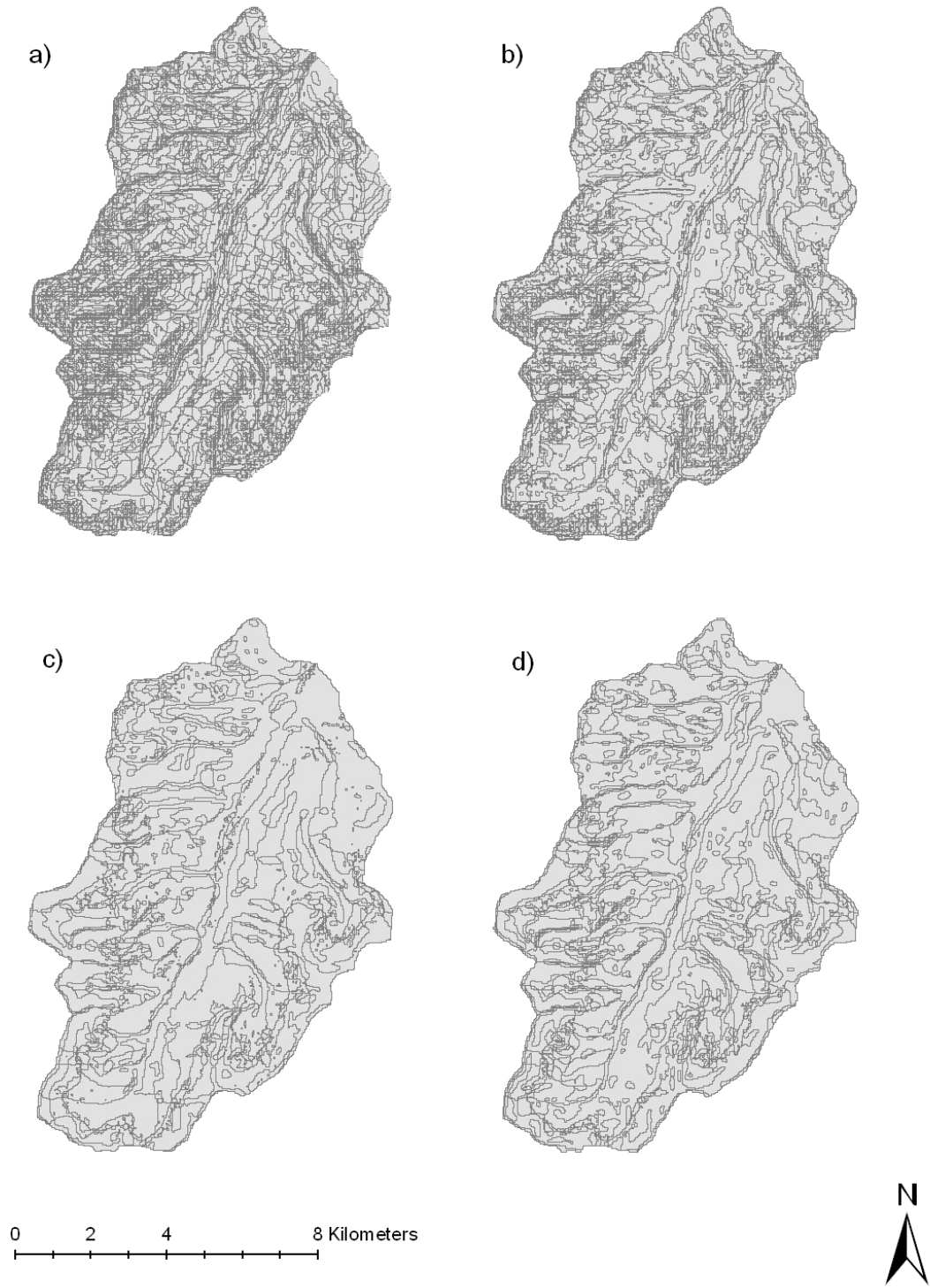


Figure 6.5. Polygon modeling units used for St. Louis Creek distributed SnowModel simulations. a) Simulation A, n=3726, b) Simulation B, n=2395, c) Simulation C, n=579 d) Simulation D, n=181

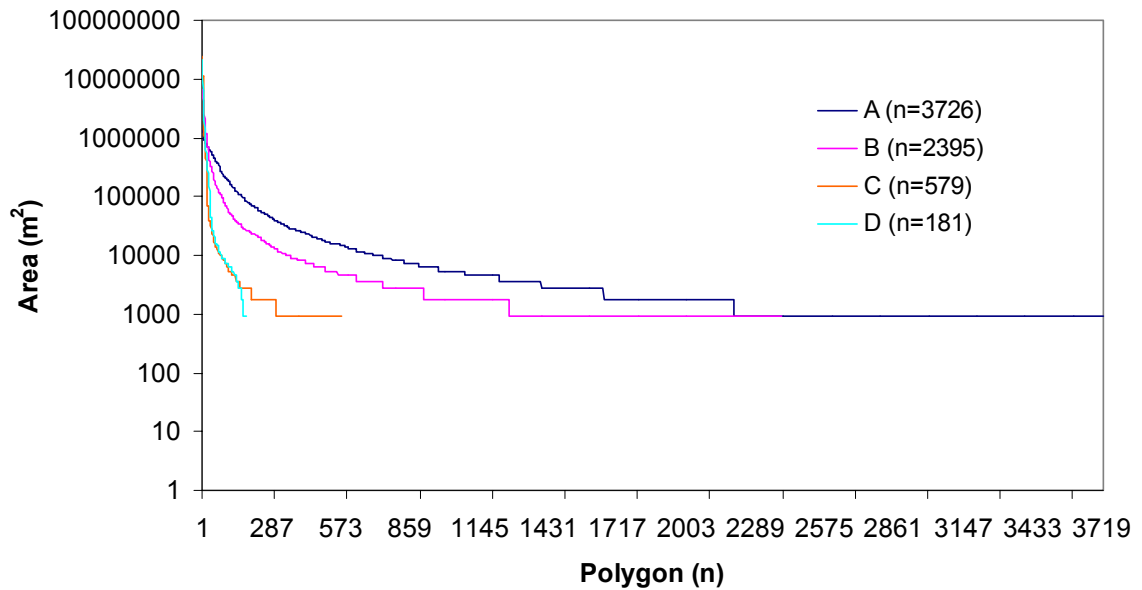


Figure 6.6. Distribution of polygon areas relative to the number of polygons in each simulation. The smallest possible modeling unit is 900m².

6.2.5 METEOROLOGICAL INPUTS

Meteorological data used for polygon simulations were derived from the dataset produced by Liston *et al.* (2007) for SnowModel grid simulations over the Fraser MSA. The data used in that study were compiled from two primary sources: meteorological station data and atmospheric analysis data. This dataset included observations from the Fool Creek and St. Louis Creek meteorological towers, along with 8 other towers installed as part of the NASA CLPX (Cline *et al.*, 2003; Elder and Goodbody, 2004). Meteorological variables collected from those towers and used to create the meteorological data for this study include wind speed and direction, air temperature and relative humidity measured from a cross-arm mounted 10 m above ground surface. Also included were data from an eddy covariance flux tower installed as part of the CLPX.

Additionally, other meteorological data was available from a variety of existing networks maintained by the USDA Forest Service, the USDA Natural Resource Conservation Service, Remote Automated Weather Stations (RAWS), and the Desert Research Institute.

Atmospheric analysis data derived from the National Oceanic and Atmospheric Administration's (NOAA) Local Analysis and Prediction System (LAPS) were also used by Liston *et al.* (2007) to compile the meteorological data which was later used in this study. During the NASA CLPX, LAPS was generated over a 10 km horizontal grid with 21 isobaric vertical levels and hourly temporal resolution. Data incorporated into the LAPS comes from a variety of sources such as surface stations, hourly surface aviation observations, Doppler radar scans, and satellite imagery. The resulting LAPS output covers Colorado, Wyoming and parts of surrounding states and includes spatially- and temporally-continuous atmospheric state variables.

Liston *et al.* (2007) used the MicroMet preprocessor (Liston and Elder, 2006a) to prepare the meteorological dataset for the simulations. MicroMet identified and filled missing values and calculated the appropriate wind speed and direction for below-canopy locations from simulated top-of-canopy wind fields.

All precipitation data used by Liston *et al.* (2007) were derived from LAPS analysis and multiplied by an adjustment factor to better predict precipitation over the MSAs. Results from an their initial SnowModel simulation over each MSA were compared to observed, and further corrections were made to the precipitation fields, based on the assumption that differences between the model and observed are largely the result of errors in the precipitation field. The adjusted precipitation correction factor

distribution over each MSA, based on SWE observations during the modeling period, was used as input for secondary and final model simulation. However, for this study, observations of SWE over the Fraser MSA during the study period were not available, and adjustments to the MicroMet precipitation fields could not be made. Therefore, the precipitation data used in this study were based only on LAPS simulations.

6.2.6 INITIAL SNOW WATER EQUIVALENT DISTRIBUTION

The SWE distribution used to initialize SnowModel was the 26 March, 2003 30 m grid SWE distribution from Liston *et al.* (2007). The SWE distributions predicted by Liston *et al.* (2007) using SnowModel were constrained by observed data assimilated into the model using the data assimilation sub-model SnowAssim (Liston and Heimstra, 2006). Ground observations of snow depth and density from the CLPX intensive study periods during February and March of 2003 (Elder and Goodbody, 2004) were used to constrain modeled SWE distributions. The 30 m grid SWE values from 26 March, 2003 were averaged over each polygon in each simulation by summing the SWE values for each cell within the boundaries of a polygon and finding the average.

6.2.7 SNOWMODEL SIMULATIONS

In order to facilitate modeling polygons on a grid system, polygon masks were created to represent the location of each polygon on the 30 x 30 km grid. Figure 6.7 is an example of how polygon masks were created for modeling. Each polygon within the basin was given a number, and the number associated with each polygon was assigned to

all 30 m grid cells that have a majority of their area within the bounds of that polygon. All cells outside of the basin were given a value of “no data” (9999).

MicroMet used the original DEM and vegetation data to simulate hourly meteorological data over each grid cell in the MSA. Once the meteorological variables were created for each grid cell, the output was summed and averaged over each grid cell in each polygon identified by the polygon mask. The result was a time series of average meteorological conditions over each HRU that were then run through SnowModel as separate modeling units. The output file for each polygon contained a time series of hourly variables over the entire modeling period, including air temperature, SWE depth, snow depth, runoff, summed runoff, incoming shortwave radiation and downwelling longwave radiation.

The time series files for each simulation were run through a Fortran program to create files for spatial display using the Grid Analysis and Display System (GrADS). Daily SWE depth, cumulative runoff and average temperature were generated as GrADS files for each polygon. Spatial displays of six days of basin-average SWE were created for each simulation using GrADS. The resulting GrADS files were processed through a to create ASCII time series outputs of basin average daily SWE depth, runoff, SCA and average daily temperature for the basin in each simulation. These results were plotted for each simulation. Additionally, a time series of daily basin average net shortwave and longwave radiation were created for simulation A for use as a comparison to observed meteorological conditions at the Fool Creek and St. Louis Creek meteorological towers.

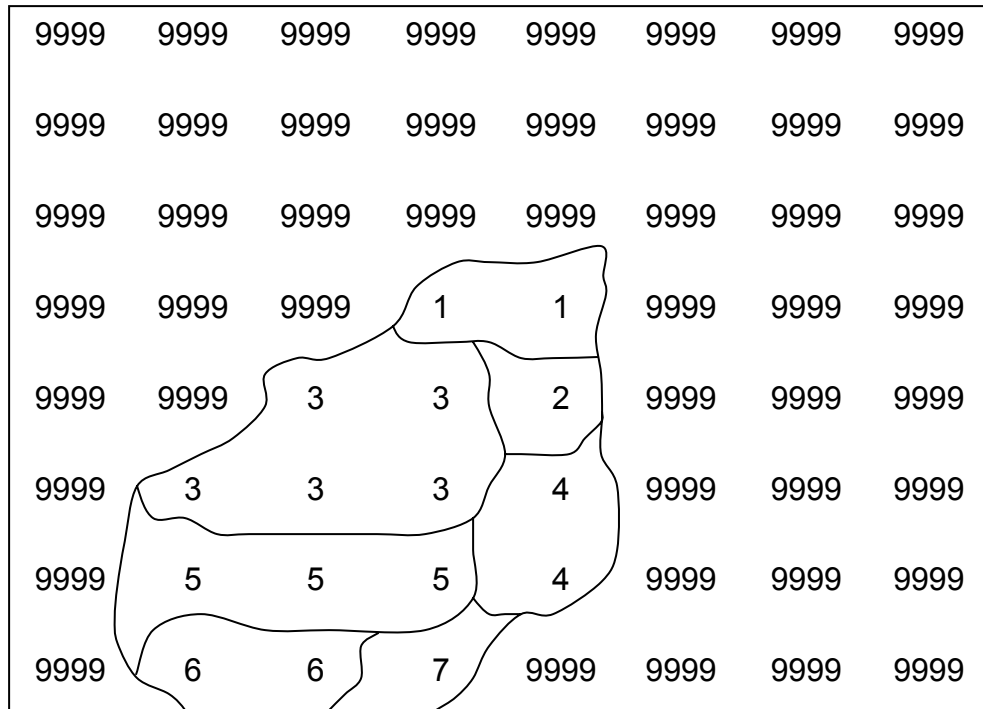


Figure 6.7. Example of polygon masks over 30 m grid cells in the Fraser MSA. Each polygon was given a unique number, and that number was assigned to all grid cells having a majority contained by that polygon. Cells outside of the basin were given a value of “no data”, or 9999.

6.2.8 ALBEDO SENSITIVITY ANALYSIS

The albedo of melting snow under a forest canopy and the albedo of snow in the open are constant, user-defined parameters in SnowModel. A sensitivity analysis of the model to varying melting snow albedos using simulation A, (n = 3726) and a literature search for appropriate melting snow albedos were conducted to determine appropriate values for all simulations (Figure 6.8).

The US Army Corps of Engineers (1956) suggested an albedo of 0.4 for a melting, 15 to 20 day old snow surface under the canopy. Link and Marks (1999) used a melting snow albedo of 0.55, after Pomeroy and Dion (1996), as the low endpoint of a melting snow albedo decay function in the boreal forest. Melloh *et al.* (2002) measured

albedo in a mixed balsam fir and white birch forest ranging from ~ 0.58 to less than 0.4 during a 10-day melt period. Hardy *et al.* (1997) reported a sub-canopy melting snow albedo of < 0.5 in a jack pine stand. It was determined that a melting snow forest albedo of 0.50 would be sufficient for the purposes of this study. An albedo of 0.60 was used for melting snow in the open (e.g. Dunne and Leopold, 1978; Male and Gray, 1981; Melloh *et al.*, 2002). These relatively high albedos were chosen based on meltout date from point simulations at Fool Creek and St. Louis Creek. Meltout from the point models was several days later than those predicted by SnowModel polygon simulations in each area, so the highest realistic albedo was used for polygon simulations to slow melting.

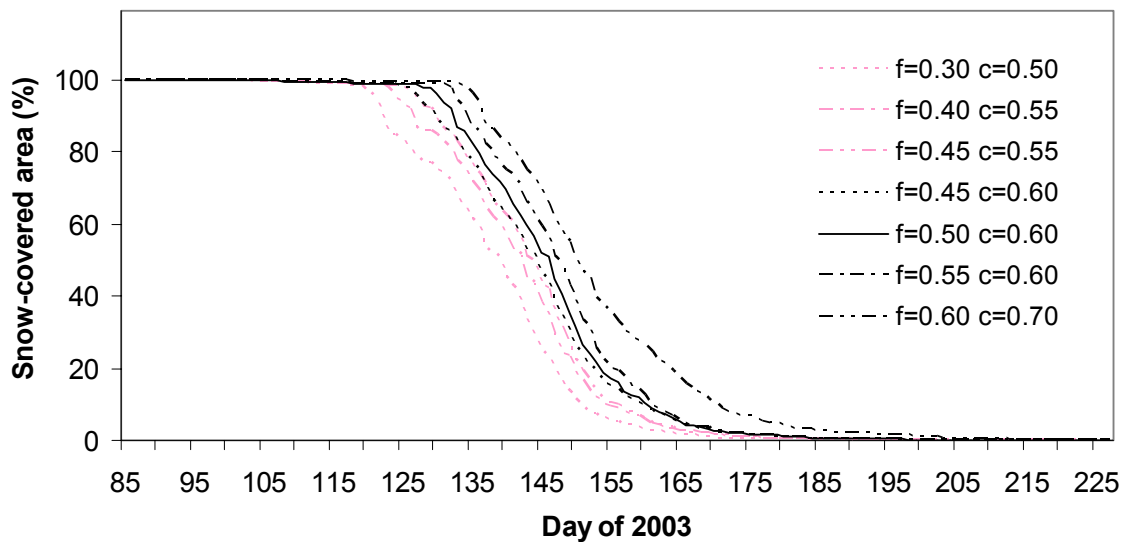


Figure 6.8. Snow-covered area depletion curves for St. Louis Creek using simulation A ($n = 3726$), with varying melting snow albedo for forested (f) and clearing (c) areas. Final albedo used in SnowModel simulations for forested areas was 0.5 and for clearings was 0.6 (solid line).

6.3 ST. LOUIS CREEK DISCHARGE RECONSTRUCTION

Denver Water installed a diversion structure in the St. Louis Creek basin in 1955 and began operations in 1956 (Carlson, 2006). The diversion structure is above the USGS gauge, and diverts flow from St. Louis Creek and neighboring Vasquez Creek before passing underneath the Continental Divide via the Moffat Tunnel (Dunford and Love, 1952). Denver Water does not record exactly how much water they remove from St. Louis Creek. Therefore, 2003 St. Louis Creek discharge measured at the USGS gauge is an underestimate of true basin runoff. East St. Louis Creek (ESL) and Fool Creek (FC) are gauged above the St. Louis Creek (STL) diversion. STL, FC and ESL were gauged simultaneously for at least 13 years prior to installation of the diversion structure in 1955 (Dunford and Love, 1952; USGS, 2006). A number of methods, including a standard autoregression model and an alternative “hydrograph method” (Porth, 2006) were applied to FC, ESL and STL pre-diversion data to derive a best estimate for 2003 STL data.

Discharge data from ESL and FC were obtained through the US Forest Service Rocky Mountain Research Station’s online data archive (Elder, 2006). STL discharge data were obtained from the US Geological Survey’s online stream database (USGS, 2006). The models were derived using data from April 23 through September 9, 1940 through 1955 for FC and STL and May 20 through September 9, 1943 through 1955 for ESL. The ESL data for 1951 ends in July rather than September, so 1951 was excluded from the autoregression model. The same procedures were followed for both ESL and FC. For clarity, only ESL data is presented as the example of methodology.

The statistics program SAS © was used to create a number of models, although some problems, such as autocorrelation and interactions between flow year (i.e. high flow

and low flow years) and daily flow points, were apparent early in the modeling process. Therefore, an autoregression model was developed using the “Proc Autoreg” function, which accounts for autocorrelation. This model was based on the equation:

$$Q_{USGS} = \alpha (Q_{ESL}) + ar1 + \varepsilon \quad (6.1)$$

where Q is average daily flow in ft^3/s , α describes the average percent contribution from ESL, $ar1$ is a single-timestep autocorrelation term (meaning only 1 timestep prior to the timestep of interest is used to establish autocorrelation), and ε is an error term. The FC model contains an $ar1$ and an $ar2$ term. Although it was determined that there was a significant ($p < 0.0001$) interaction between flow year and daily flows, the model output and error reduction from the interaction model was not enough to justify using a more complex model. However, since the residuals lacked normality and homogeneous variance, an alternative method was derived.

The “hydrograph method” uses each data point’s position on the spring/summer hydrograph as a percentage of cumulative daily flow (cdf) to predict the average value for 2003 STL discharge. First, the ratio of STL/ESL flow was calculated for each day of each year (including STL 1951). Then, the position of each day on the hydrograph was determined by calculating the cumulative daily flow throughout each year and calculating what percentage of the cdf was achieved each day. The percentage of flow was rounded to the nearest 1%, so during a 153 day runoff season, more than one day of discharge fell on a single percent value, such as 1%, 1% and 2% for the first three values of the year. Then, the average discharge ratio (STL/ESL) for each one percent of each year was

calculated (i.e. if there were two “3%” values, the ratios for those two days were averaged to produce a single ratio for that percent value for that year). The same method was used to find where on the hydrograph each day in 2003 fell for ESL (1-100). Each day of flow with the same percentage in 2003 was then multiplied by each year’s average STL/ESL ratio for the same percentage, i.e. the actual daily discharge for every 1% of ESL cumulative daily flow in 2003 was multiplied by the average STL/ESL ratio for 1% of the cdf for each year to produce an estimate of what flow would be in 2003 using each year’s ratio. This produced up to 13 values of flow, one prediction for each year 1943-1955, for each day in 2003 (Figure 6.9). Average and median values were calculated for each day. This method eliminates concern with autocorrelation and non-homogeneous variance. Figure 6.10 displays daily flow predictions using both modeling methods for both drainages.

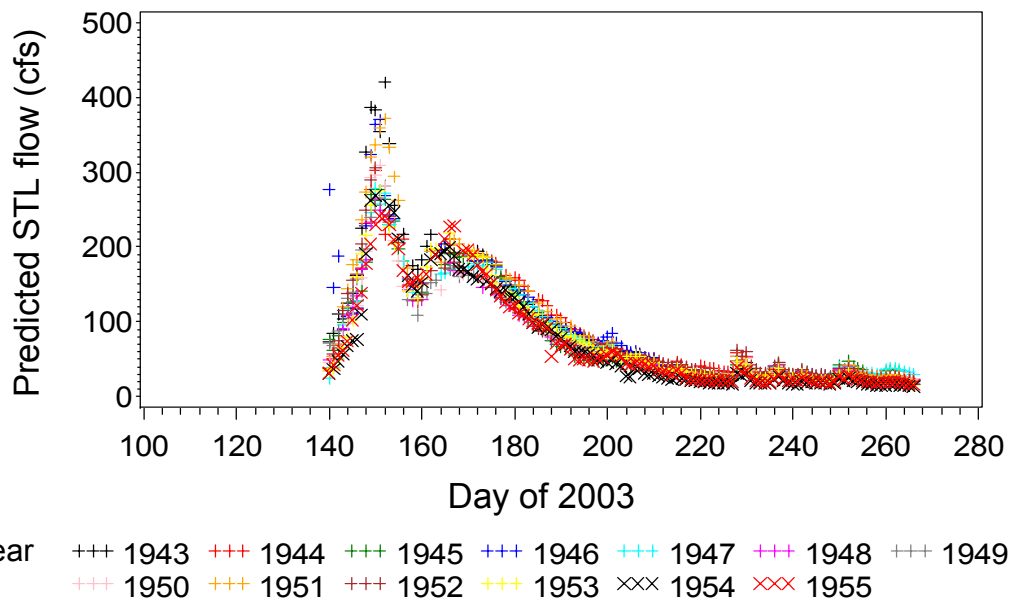


Figure 6.9. Results of hydrograph method of daily flow prediction for St. Louis Creek using East St. Louis Creek discharge from 1943 – 1955. Each marker represents one day of data for each model year. Each day in 2003 has up to 13 predictions, one derived from each year of pre-diversion data.

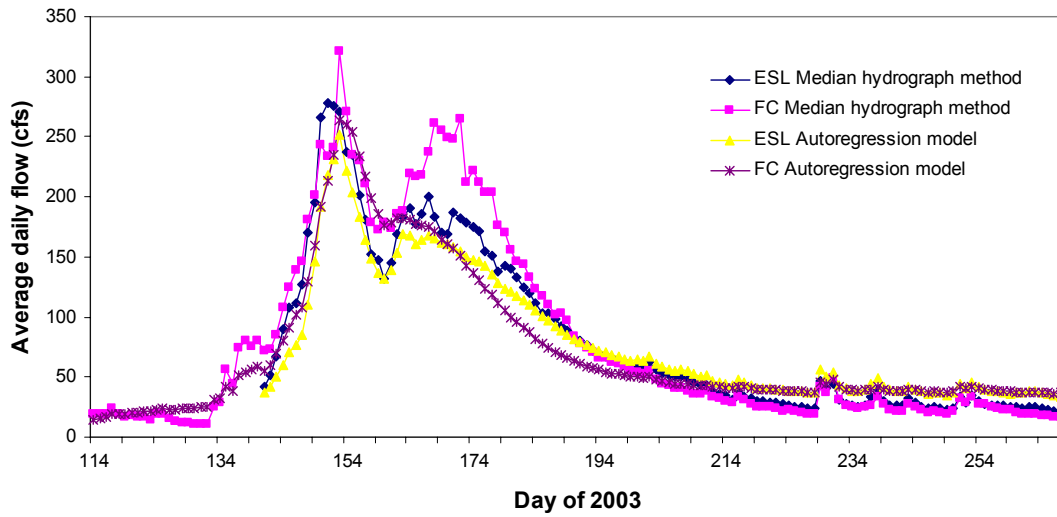


Figure 6.10. Predicted 2003 St. Louis Creek discharge using pre-diversion data from Fool Creek (1940 – 1955) and East St. Louis Creek (1943 – 1955) and two prediction methods.

Annual flow was calculated using a normal regression model in SAS. It was determined that autocorrelation between years, although present, was not significant so the simpler regression model was used. This model was of the form:

$$Q_{USGS} = \alpha (Q_{ESL}) + \varepsilon \quad (6.2)$$

where Q is cumulative annual flow in ft^3/year , α describes the average percent contribution from ESL, and ε is an error term. Annual flow was also calculated from the sum of predicted daily flows from both methods. Table 6.5 displays annual flow results from all methods. All annual flow predictions using ESL were within 95% of each other. All annual flow predictions using FC were within 88% of each other, with the autoregression model sum being the lowest.

Table 6.5. Predicted annual flow at East St. Louis Creek and Fool Creek derived from the modeling period 1940 – 1955 for Fool Creek and 1943 – 1955 for East St. Louis Creek. Summed values are cumulative flow derived from modeled daily flow predictions.

Prediction method	ESL Predicted cumulative flow (ft³/yr)	FC predicted cumulative flow (ft³/yr)
Hydrograph median (sum)	10647	12395
Hydrograph average (sum)	10814	12585
Autoregression model (sum)	10376	11116
Regression model	10875	12132

In the final step, all methods were graphically compared to gauged 2003 STL discharge. Although using ESL as a predictor had the lowest statistical error (Table 6.6), it is possible that using FC as a predictor actually predicted 2003 STL discharge best by predicting a larger second peak. The observed STL discharge at the USGS gauge is shown in Figure 6.7 along with FC and STL hydromethod-predicted discharge. Because of the diversions, the observed discharge may or may not have been an underestimate at any point, but at all points where observed STL discharge was greater than predicted discharge, it was likely that the predicted values were underestimated (i.e. days 174-183). Therefore, both ESL hydromethod and FC hydromethod were used to reconstruct estimated 2003 STL discharge, and both were used to develop depletion curves for 2003 snowmelt runoff.

Table 6.6. Root mean square error values for St. Louis Creek 2003 daily flow predicted using an autoregression model and a hydrograph estimation method for Fool Creek (1940 – 1955) and East St. Louis Creek (1943 – 1955).

Model	FC RMSE (cfs)	ESL RMSE (cfs)
Proc Autoreg ar1	19.42	12.24
Proc Autoreg ar2	18.45	-
Hydrograph Method	11.21	8.29

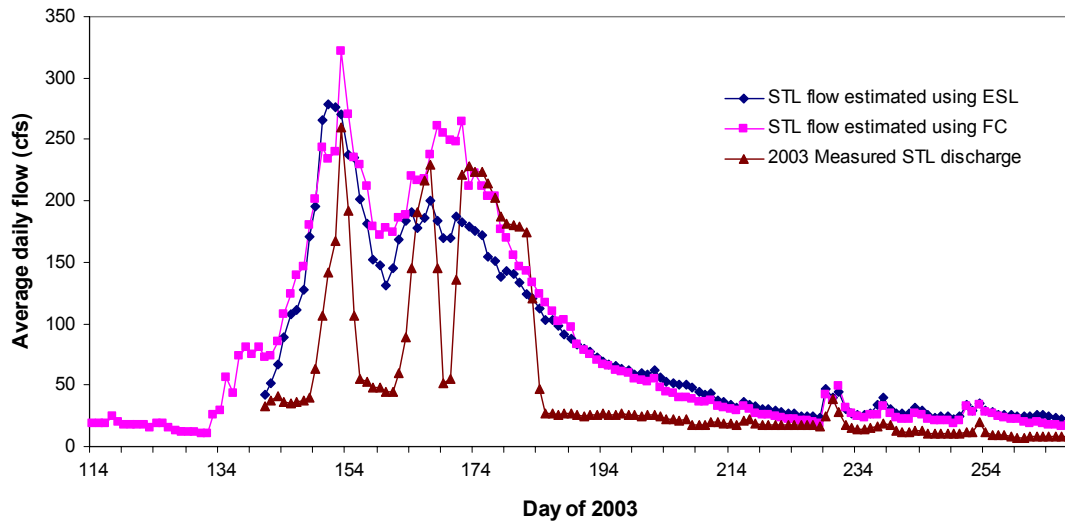


Figure 6.7. Predicted 2003 St. Louis Creek discharge using pre-diversion data from Fool Creek (1940 – 1955) and East St. Louis Creek (1943 – 1955) using the hydrograph method and observed 2003 St. Louis Creek discharge.

6.4 SNOW-COVERED AREA DEPLETION CURVES

Two types of empirical depletion curves were created for all simulations using the time series of SCA: one was depletion of snow cover as a function of time and the other was depletion of snow cover as a function of reconstructed cumulative runoff, as per USACE (1953; 1956).

6.5 STATISTICAL ANALYSES OF POINT MODEL RESULTS

Point model results were evaluated by calculating the Nash-Sutcliffe coefficient (NS), root mean square error (RMSE), and mean bias error (MBE). The Nash-Sutcliffe coefficient was calculated using:

$$NS = 1 - \frac{\sum (x - x_o)^2}{\sum (x_o - x_m)^2} \quad (6.3)$$

where x is modeled snow depth (m), x_o is observed snow depth (m), and x_m is mean observed snow depth (m). The RMSE was calculated using:

$$\text{RMSE} = \sqrt{\frac{\sum (x - x_o)^2}{n}} \quad (6.4)$$

where n is the number of observations, and MBE was calculated using:

$$\text{MBE} = \frac{\sum (x - x_o)}{n} \quad (6.5)$$

6.6 STATISTICAL ANALYSES OF DISTRIBUTED MODEL RESULTS

Spatial distributions of SWE and temperature were visually compared using GrADS displays. Summary statistics of basin-wide results SCA and SWE were calculated similarly to those for the point models, using the Nash-Sutcliffe coefficient (Equation 6.3) to compare model results only to each other, since no observations are available for a rigorous statistical analysis. Time series of SCA, SWE and temperature were also compared using visual estimates of graphical results.

CHAPTER 7. RESULTS AND DISCUSSION

7.1 POINT SIMULATIONS

7.1.1 FOOL CREEK

Point estimate results for snow depth and snow water equivalent (SWE) at Fool Creek are shown in Figure 7.1. Results were split into an accumulation period when snowfall was occurring (24 March through 10 May) and an ablation period when snow accumulation had ceased and the snowpack depleted (10 May through 3 June). The entire modeling period from 24 March through 3 June, 2003 was 71 days in length.

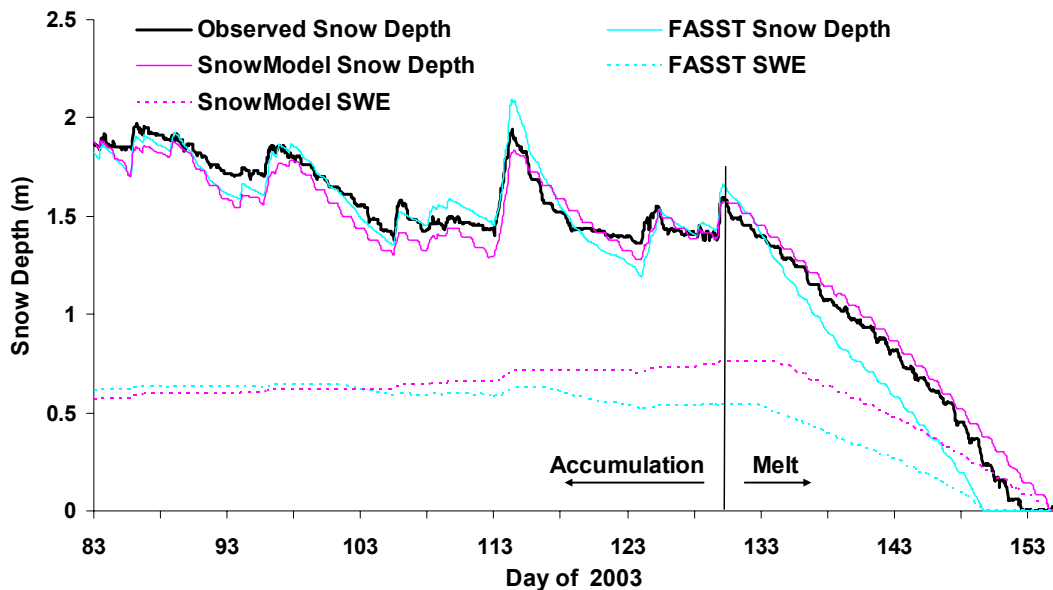


Figure 7.1. SnowModel and FASST hourly snow depth and SWE predictions and observed snow depth at Fool Creek meteorological tower, 24 March through 3 June, 2003. Accumulation period is 24 March through 10 May and melt period is 10 May through 3 June.

The high Nash-Sutcliffe coefficients and low root mean square error and mean bias error for both FASST and SnowModel snow depth predictions for all modeling periods (Table 7.1) indicate that both models successfully predicted timing and magnitude of changes in snow depth. Observed total snow depletion occurred on day 152 at 15:00 MST. FASST predicted complete ablation on day 150 at 23:00 MST, 40 hours prior to observed melt, and SnowModel predicted complete ablation on day 154 at 23:00 MST, 50 hours after observed melt. Although both models did an excellent job simulating late season snow depth, SnowModel performed slightly better than FASST overall and during the ablation period and FASST performed better than SnowModel during the accumulation period. Both models predicted similar SWE through day 105, after which SnowModel predicted a denser snowpack than did FASST.

Table 7.1. 2003 SnowModel and FASST performance results at Fool Creek meteorological tower for 24 March through 3 June (overall), 24 March through 10 May (accumulation) and 10 May through 3 June (ablation). Nash-Sutcliffe coefficient (N-S), root mean square error (RMSE) and mean bias error (MBE) were used to evaluate the models' performance.

	Overall		Accumulation		Ablation	
	<i>FASST</i>	<i>SnowModel</i>	<i>FASST</i>	<i>SnowModel</i>	<i>FASST</i>	<i>SnowModel</i>
N-S	0.95	0.97	0.84	0.78	0.87	0.97
RMSE (cm)	0.12	0.08	0.07	0.09	0.17	0.08
MBE (cm)	-0.05	-0.01	-0.01	-0.06	-0.13	0.07

Some of the variation between SnowModel and FASST snow depth and SWE predictions can be explained by differences in the models themselves. For example, SnowModel calculates compaction due to the weight of the overlying snow (overburden) and compaction due to melt. FASST calculates compaction due to overburden and water in the snowpack similar to SnowModel, but it also calculates densification of snow due to

snow metamorphism based on temperature, density of water in the frozen state and the fraction of the snowpack which is wet. The compaction calculated by SnowModel during the “accumulation” season was more linear following precipitation events, whereas the compaction calculated by FASST was slightly curved, likely due to additional compaction calculated from snow metamorphism following new snow accumulation. This trend was particularly noticeable following precipitation on days 114-115 in Figure 7.1. Differences between FASST and SnowModel SWE increased following precipitation events, indicating that the ways in which each model calculated compaction influenced SWE calculations, with SnowModel predicting greater snow density than FASST.

Another difference between FASST and SnowModel is the calculation of new snow density (ρ_{ns}) from incoming precipitation. Both models calculate new snow density based on temperature, but SnowModel uses a temperature dependency calculation after Anderson (1976) and FASST uses a calculation after Jordan *et al.* (1999), which is a function of both temperature and wind speed. Typically, each model calculated a different new snow depth for each precipitation event. Incoming precipitation at Fool Creek for both models was identical and given in millimeters of water equivalent. Snow depth was adjusted at each timestep according to the calculated new snow density. FASST calculated greater increases in snow depth following nearly every precipitation event, as shown in Figure 7.1, due to lower calculated snow density. Although differences in model-predicted SWE are less pronounced, the precipitation event on day 115 resulted in a greater snow pack density predicted by SnowModel, as indicated by a greater increase in SWE and lesser increase in snow depth relative to those predicted by

FASST. It is possible that faster final melt of the snowpack predicted by FASST is a result of underestimated SWE.

Another significant difference between FASST and SnowModel is the calculation of snow albedo. SnowModel uses a constant albedo, which is either 0.8 for non-melting snow, or user-defined values for melting snow. Melting snow albedo is defined for snow in forested areas and snow in non-forested areas to account for factors such as litter accumulation on the snowpack in forested areas. FASST calculates snow albedo at each timestep using one of three methods (refer to Chapter 5, section 5.1). The albedo calculated by FASST was often less than 0.5 during the final melt phase. The constant melting snow albedo in SnowModel was defined to be 0.5. SnowModel depleted more slowly than FASST during the final melt, likely due to higher albedo, and had a more linear depletion pattern. This is most obvious during the “melt” period in Figure 7.1.

7.1.2 ST. LOUIS CREEK

Point estimate results for snow depth at St. Louis Creek are shown in Figure 7.2. Statistical analyses of results are presented in Table 7.2. Again, results were split into an accumulation period (27 March through 10 May) and an ablation period (10 May through 22 May). Total modeling period from 27 March through 22 May, 2003 is 56 days in length.

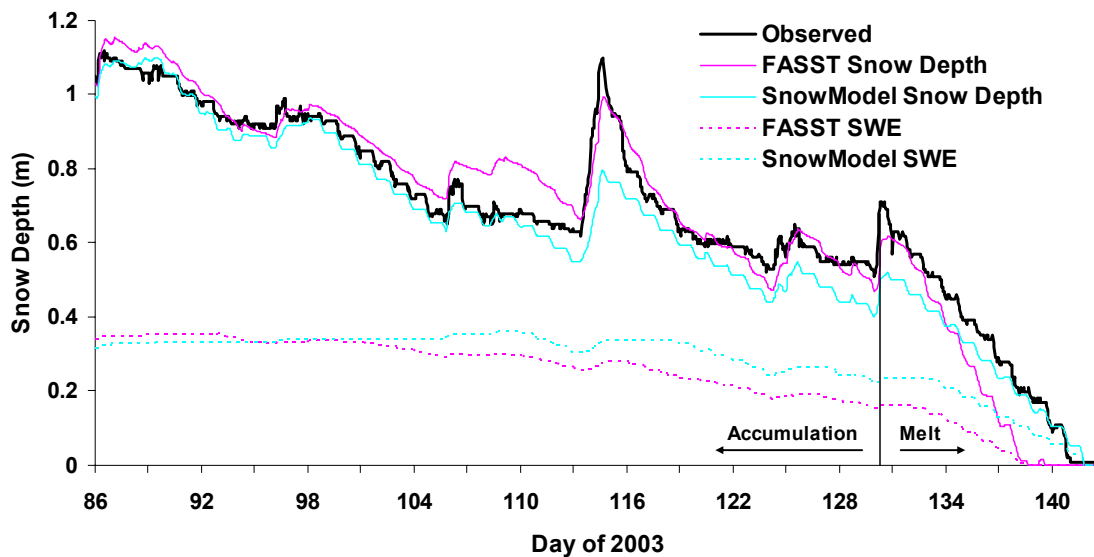


Figure 7.2. 2003 SnowModel and FASST hourly snow depth and SWE predictions and observed snow depth at St. Louis Creek meteorological tower, 27 March through 22 May, 2003. Accumulation period is 27 March through 10 May and melt period is 10 May through 22 May.

The high Nash-Sutcliffe coefficients and low root mean square error and mean bias error for snow depth predicted by both FASST and SnowModel for all modeling periods (Table 7.2) indicate that both models successfully predicted timing and magnitude of changes in snow depth. Both models predicted meltout within 36 hours of observed depletion. Observed total snow depletion occurred on day 140 at 19:00 MST. FASST predicted complete ablation on day 139 at 07:00 MST, which is 36 hours prior to observed meltout. SnowModel predicted complete ablation on day 141 at 13:00 MST, which is 18 hours after observed meltout. SnowModel slightly underpredicted snow depth for the latter half of the accumulation season, and FASST overpredicted snow depth during days 106-114. SnowModel predicts greater snowpack density than FASST for the modeling period after day 100.

Table 7.2. 2003 SnowModel and FASST performance results at St. Louis Creek for 27 March through 22 May (overall), 27 March through 10 May (accumulation) and 10 May through 22 May (ablation). Nash-Sutcliffe coefficient (N-S), root mean square error (RMSE) and mean bias error (MBE) were used to evaluate the models' performance.

	Overall		Accumulation		Ablation	
	<i>FASST</i>	<i>SnowModel</i>	<i>FASST</i>	<i>SnowModel</i>	<i>FASST</i>	<i>SnowModel</i>
N-S	0.92	0.92	0.89	0.82	0.70	0.86
RMSE (m)	0.07	0.07	0.06	0.07	0.11	0.07
MBE (m)	0.00	-0.05	0.03	-0.05	-0.10	-0.06

Again, variations between FASST and SnowModel outputs were likely a result of differences between the models, as mentioned above. FASST calculated a lower new snow density for the precipitation events on days 106 and 108, leading to an overestimate of snow depth relative to observed and to SnowModel (Figure 7.2). It is also possible that SnowModel overestimated new snow density for the storm on day 113, leading to an underestimate of snow depth. Decreases in albedo and compaction calculations were likely responsible for variations in snowpack depletion rate and timing as predicted by each model, similar to patterns discussed for Fool Creek. Additionally, it is possible that incoming precipitation was misrepresented by the models at this site due to the precipitation gauge being located 2.6 km southwest of the meteorological tower. There may be differences in precipitation between these two sites that influenced model-predicted versus observed snow depth. It is possible that an underestimation of SWE led to early melt and faster melt rate predicted by FASST and an overestimation of SWE led to a slower melt rate predicted by SnowModel

7.2 POLYGON MODEL SIMULATIONS

7.2.1 SNOW WATER EQUIVALENT DEPLETION

The average basin SWE for the modeling period for each simulation is shown in Figure 7.3. The lack of snow depth variability and modeling units contributed to earlier meltout in simulation E (basin average). Although basin average SWE is similar for simulations A-D, there is some difference between the high polygon number simulations (A and B) and the low polygon number simulations (C and D), such as greater SWE in A and B from approximately day 138 through day 151. It is likely a function of increased spatial variability in simulations A and B that the duration of SWE depletion is longer and basin average SWE is slightly greater in magnitude.

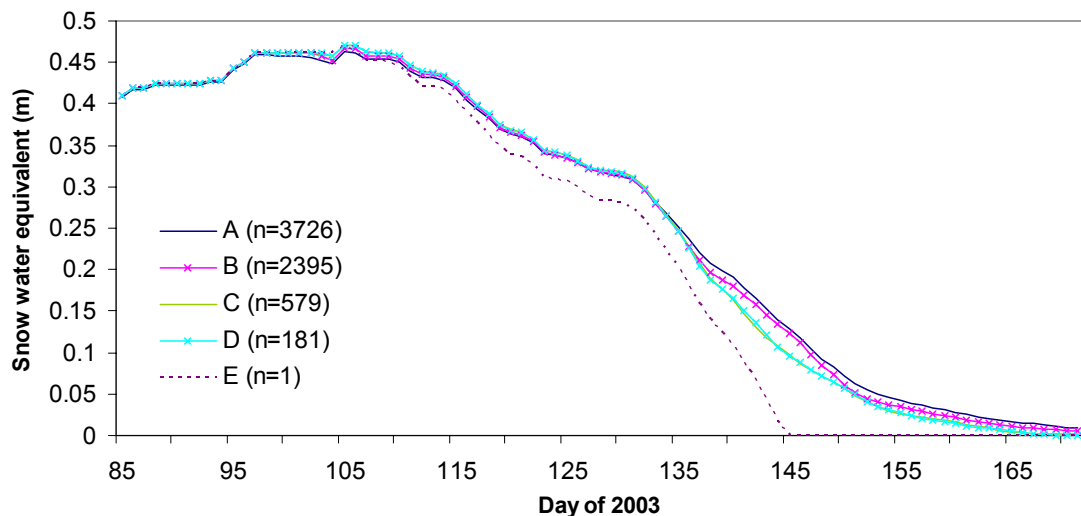


Figure 7.3. Average basin SWE depletion versus time for each of five SnowModel simulations for the period of 27 April through 3 July, 2003 in St. Louis Creek basin. “n” is the number of polygons in each simulation.

Daily average SWE results for simulations B-E were compared to simulation A, which was used as the “control”. Results of statistical comparisons of simulation A to

simulations B-E are given in Table 7.3 only for the purpose of estimating the differences between simulations, not as a rigorous statistical analysis of results. The high Nash-Sutcliffe and low RMSE and MBE values for all simulations indicate that there is little difference between simulations. Simulation B was most similar to simulation A, with the highest Nash-Sutcliffe and lowest RMSE and MSE and simulation E had the lowest Nash-Sutcliffe and highest RMSE and MBE. The comparisons between simulations indicate that the modeled predictions of basin-average SWE are not sensitive to this particular division of HRUs in St. Louis Creek. All simulations were initiated using the same SWE distribution, and although the initial distribution of SWE was different for each simulation, the overall basin-average SWE was not. The similar rate, timing and magnitude of change in basin-average SWE indicates that the amount of energy coming into the basin is the same for all simulations.

Table 7.3. Comparison depletion results for St. Louis Creek basin for 26 March through 29 July. Nash-Sutcliffe coefficient (N-S), root mean square error (RMSE) and mean bias error (MBE) were used to compare simulations B-E to simulation A.

	B	C	D	E
N-S	0.999	0.997	0.997	0.959
RMSE (m)	0.005	0.011	0.011	0.037
MBE (m)	-0.002	-0.004	-0.004	-0.022

Spatial distribution of basin SWE for six days during the melt period for simulations A-D are shown in Figures 7.4-7.7. These six days (May 14, 18, 22, 26, 30 and June 2, 2003) were chosen based on three factors: 1) days where SWE distributions differed greatly between simulations; 2) periods where large changes in SWE took place; and 3) finding a relatively even distribution of days over the melt season.

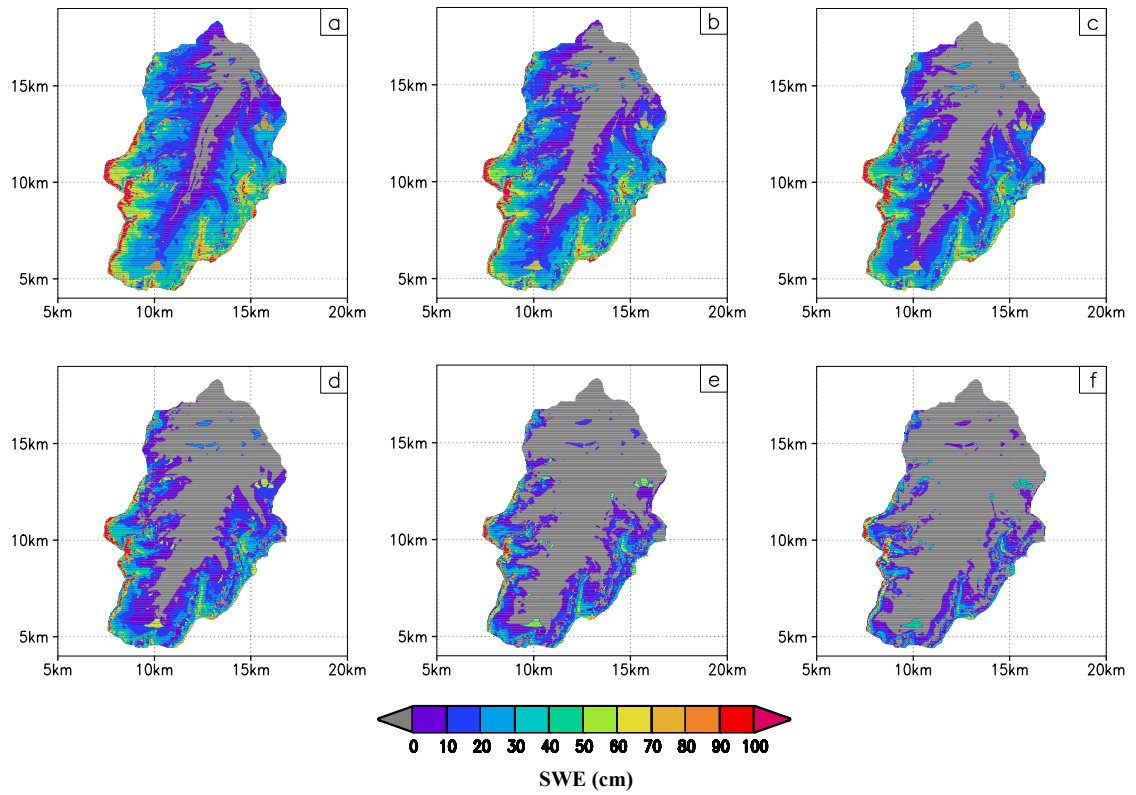


Figure 7.4. Simulation A (n=3726) spatial distribution of SWE over St. Louis Creek Basin for six days in 2003. Days are as follows: a) May 14, b) May 18, c) May 22, d) May 26, e) May 30 and f) June 2

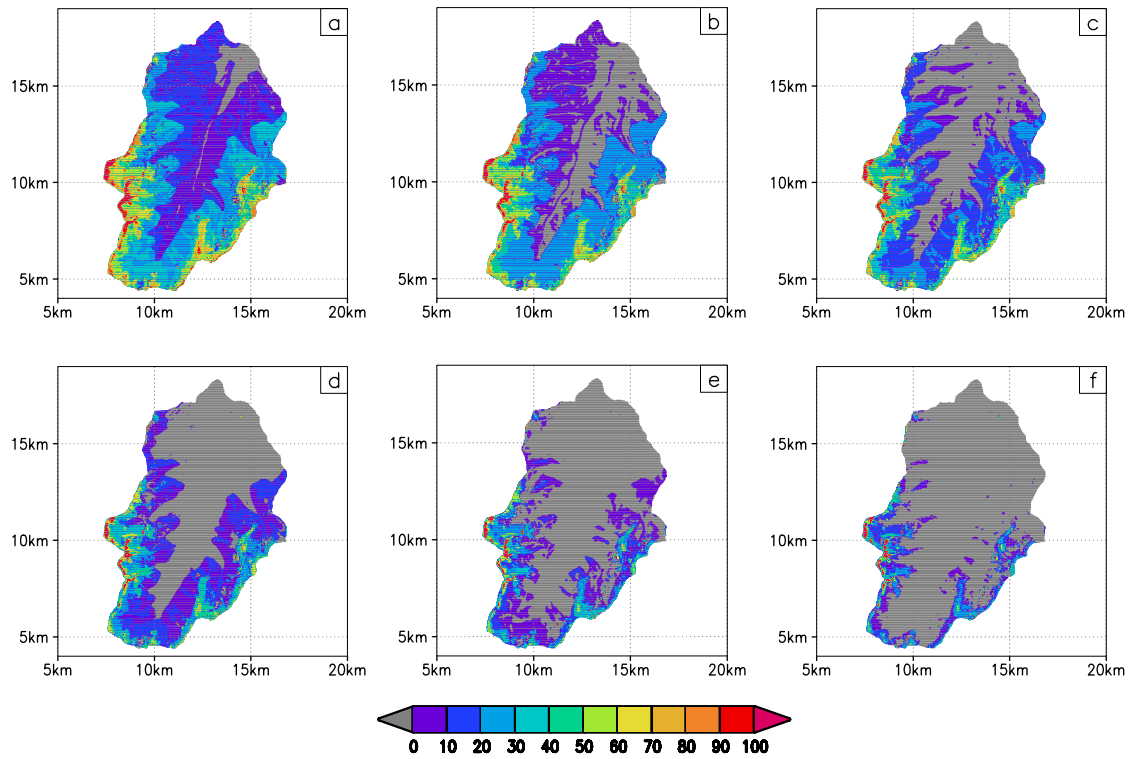


Figure 7.5. Simulation B (n=2395) spatial distribution of SWE over St. Louis Creek Basin for six days in 2003. Days are as follows: a) May 14, b) May 18, c) May 22, d) May 26, e) May 30 and f) June 2

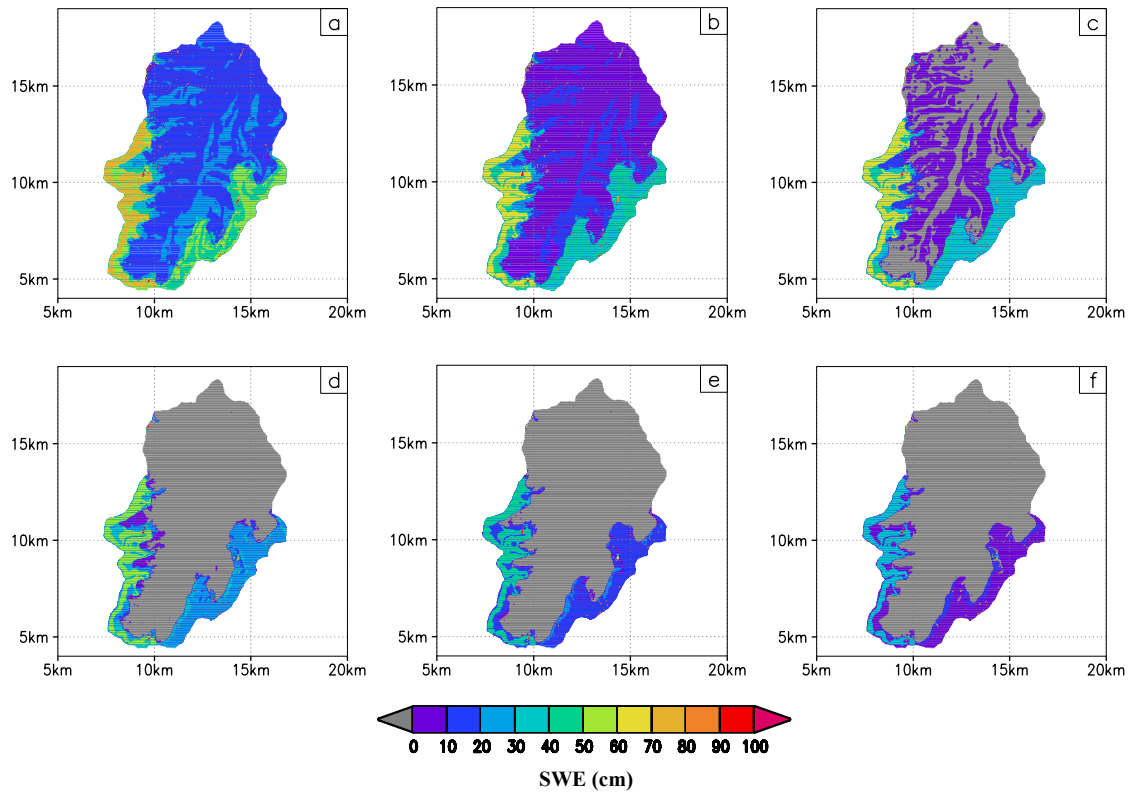


Figure 7.6. Simulation C (n=579) spatial distribution of SWE over St. Louis Creek Basin for six days in 2003. Days are as follows: a) May 14, b) May 18, c) May 22, d) May 26, e) May 30 and f) June 2

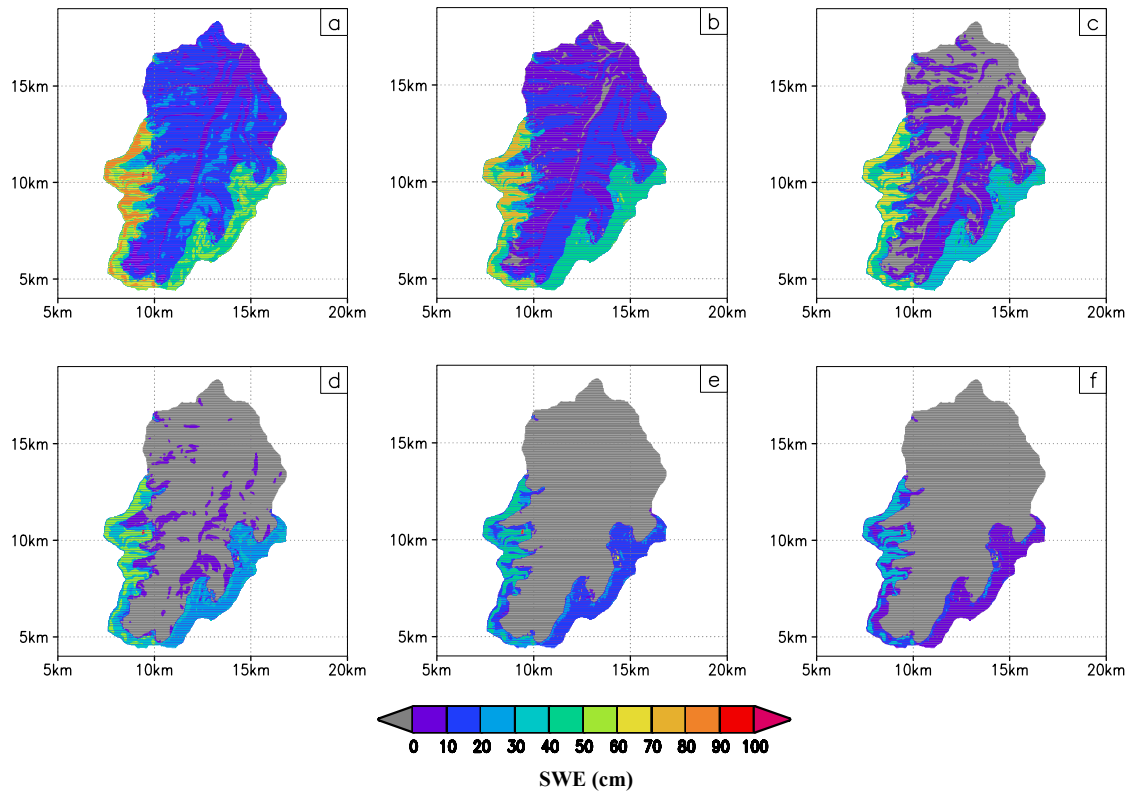


Figure 7.7. Simulation D (n=181) spatial distribution of SWE over St. Louis Creek Basin for six days in 2003. Days are as follows: a) May 14, b) May 18, c) May 22, d) May 26, e) May 30 and f) June 2

It is likely that the most important factor governing the distribution of SWE through the basin in every simulation was the starting SWE distribution from Liston *et al.* (2007). Liston *et al.* (2007) state that the SnowModel SWE distribution results for their study areas, including the Fraser MSA and St. Louis Creek basin are a good estimate of 2003 snow distributions in the complex landscapes of north-central Colorado and that the representations of SWE distributions in these landscapes are highly realistic. However, there is uncertainty in the exact distribution and magnitude of SWE due to the uncertainty and error in data collection and model output. Ultimately, the initial SWE distribution used in this study is an excellent starting point, but the results of this study are skewed toward any bias inherent in the SWE distribution from Liston *et al.* (2007). Additionally, using data such as remote sensing of SCA or SWE to force results closer to reality was beyond the scope of this study. Yet, the distribution of SWE and timing and magnitude of depletion was realistic according to known factors affecting snowpack depletion such as aspect, slope, elevation and vegetation cover (i.e. the lowest elevation polygons depleted first in all simulations).

Results from simulations A and B (Figures 7.3 and 7.4) are similar, with the effect of polygon averaging being more visible in Figure 7.4. Simulation A, which has approximately 1/3 more polygons than simulation B, better represents extremes in SWE distribution, i.e. more smaller polygons in the lowest and highest portions of the basin reflect the areas with very little (or zero) SWE and areas with large SWE, respectively. These areas of extreme lows and highs decrease as the polygon sizes increase and the area over which the initial 30-m SWE distribution is averaged. Overall, both simulations

A and B display a potentially realistic representation of SWE depletion where changes are less abrupt and the progression of melt in the basin happens more slowly.

Results from simulations C and D (Figures 7.5 and 7.6) display patterns of depletion with little spatial variability across the basin and large tracts of land showing nearly identical SWE at the same time. Snow depletion happens at a more rapid rate, which is largely a function of the averaging of initial SWE distribution over fewer, large polygons and the loss of extreme highs and lows of SWE. There does not appear to be substantial differences in SWE distribution between these simulations despite the fact that simulation C has about four times more polygons than simulation D. However, the general depletion pattern in the basin is realistic (i.e. low elevations depleting first), even if the timing and magnitude are not.

Overall, these results indicate that while the model is not sensitive to how the basin is divided up when predicting basin-average SWE, it is sensitive to the distribution of modeling units and the averaging of initial snow distribution when predicting SWE distribution throughout the basin.

7.2.2 SNOW-COVERED AREA DEPLETION

Snow-covered area (SCA) depletion curves for simulations A-E are shown in Figure 7.8. The duration of melt (from ~99.5% SCA to ~1% SCA) was 61, 52, 48, and 45 days for simulations A-D, respectively. Overall, SnowModel predicted the smoothest depletion curve at the finest spatial resolution (Simulation A) (Figure 7.8). Depletion from individual polygons is binary (snow/no snow). Therefore, the basin average SCA value (simulation E) depleted instantaneously and at the approximate midpoint of the

depletion curves for the other simulations. That the length of depletion is longer in simulations with more polygons is a reflection of: 1) the averaging of initial SWE distribution throughout the basin and the ability of finer resolution modeling units to better represent areas of extreme high and low SWE; and 2) how fine spatial resolutions best represent the spatial and temporal heterogeneity in snow cover depletion that occurs on the ground.

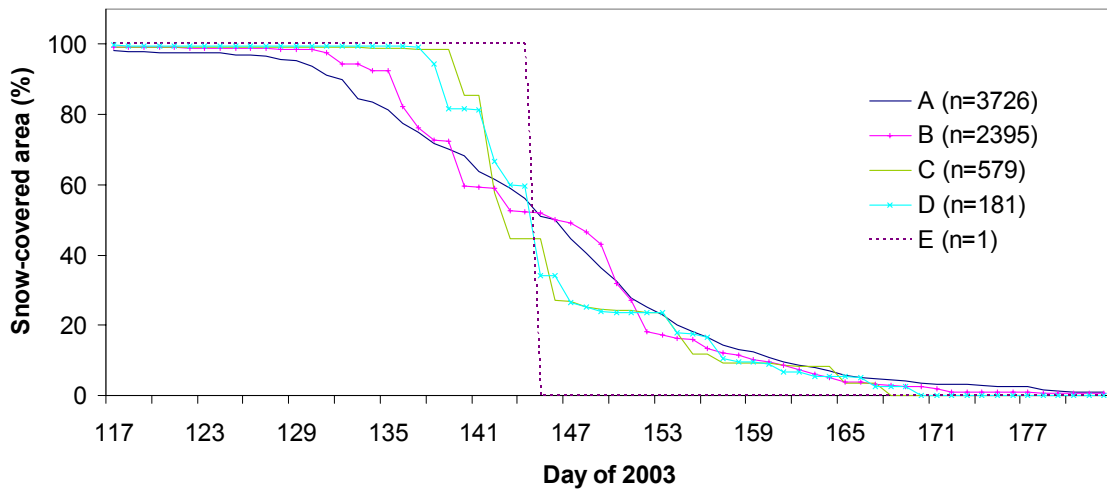


Figure 7.8. Snow-covered area depletion versus time for each of five SnowModel simulations for the period of 27 April through 3 July, 2003 in St. Louis Creek basin. “n” is the number of polygons in each simulation, and snow cover for each polygon is binary (snow/no snow).

Simulations A and B have similar depletion patterns, with B being coarser than A, but generally following a similar path of melt timing and magnitude. There are some large drops in SCA in simulation B, likely due to high numbers of polygons with similar characteristics melting out at the same time. It is possible that melt in simulation B is skewed by singular polygons with large area depleting, although this scenario is more likely seen in simulations C and D, where fewer polygons of larger area will have a

greater effect on melt rate and timing. Simulations C and D have similar depletion patterns, but the distribution of polygons in the basin creates large amounts of melt at slightly different times.

The increasing size of the modeling units creates a later start to the melt season and a shorter overall length of melt, largely due to the initial SWE distribution in each simulation. Figure 7.9 shows differences in dates at which each simulation reaches various levels of snow-covered area. As the initial distribution of SWE is averaged over larger areas, high and low extremes of snow cover are attenuated, leading to a later start and earlier finish to the melt season. In the middle stages of SCA, the physiographic properties of the basin are better represented by all simulations due to average values of large polygons being similar to those of small polygons in the mid-elevation portions of the basin. At less than 5% SCA, spread in dates increases to nearly 10 days (not shown) again as a result of decreased representation of spatial heterogeneity in melt at high elevations in simulations C and D.

If depletion curves C and D shown in Figure 7.8 represented actual predicted melt in this basin, the implication would be that large areas of land become snow-free instantaneously. This is likely not reflective of the actual physical properties in the basin. Snow-cover depletion curves in areas where the scale of spatial heterogeneity of the landscape is greater than the modeling scale, such as in simulations A and B, are likely to be similar to the smooth, gradual curves generated by A and B and basins with greater variability in terrain show longer, continuous depletion curves (e.g. Leaf, 1969; Hendrick *et al.*, 1971; Liston, 1999). Therefore, curves A and B seem to be the most realistic, although they are still simulations, not observations. Results of statistical comparisons of

simulation A to simulations B-E are given in Table 7.3 only for the purpose of estimating the differences between simulations. Statistics were calculated for the days between ~99.5% SCA through ~1% SCA in simulation A.

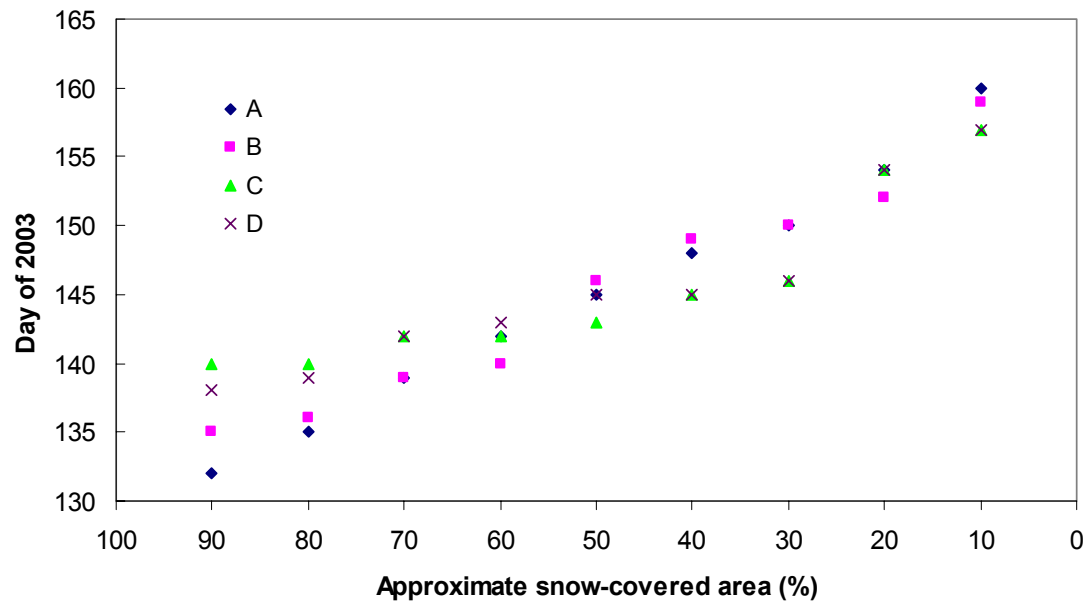


Figure 7.9. Day in 2003 at which approximate modeled values of snow-covered area are reached in the St. Louis Creek basin for simulations A-D, 10 May through 14 June, 2003.

Table 7.4. Comparison of SCA depletion results for St. Louis Creek basin for 20 April through 1 July, 2003. Nash-Sutcliffe coefficient (N-S), root mean square error (RMSE) and mean bias error (MBE) were used to compare simulations B-E to simulation A.

	B	C	D	E
N-S	0.995	0.965	0.973	0.852
RMSE (%)	3.508	9.233	8.134	19.090
MBE (%)	0.191	0.768	1.084	-1.429

The high root mean square error (RMSE) for simulation E (19.090%) indicates that simulation E did not compare favorably to simulation A, despite a relatively high

Nash-Sutcliffe value (0.852). Simulations C and D had RMSEs that were within 10% of simulation A and high Nash-Sutcliffe values. Simulation B was very similar to simulation A, with a very high Nash-Sutcliffe value and low RMSE and MBE.

Figure 7.10 shows the average depth of SWE across all areas that are snow-covered. The peaks in Figure 7.10 represent days during which large areas with relatively shallow snow became snow-free, leaving smaller areas to compensate for a similar amount of basin SWE and skewing the remaining basin SWE to greater average depths. The peaks decrease over a number of days, representing a depletion of the snowpack over the remaining polygons, until some polygons become snow free and the cycle starts over.

The smoothest curve is simulation A, where there are increased numbers of smaller polygons melting out at a somewhat sustained rate, leading to less dramatic peaks in SWE depth over remaining SCA. Although it appears that there was still a large amount of SWE at the end of the melt period, in reality there were deep drifts remaining only in very few polygons.

Figure 7.11 shows the amount of snow-covered area in the basin related to the percentage of overall SWE that has ablated. The relationship between decreasing SWE in polygons and complete ablation is visible in Figure 7.11. There are many places, particularly in simulations C and D, where a decrease in SWE was not accompanied by a decrease in SCA, until suddenly there was a decrease in SCA as large polygons or many polygons simultaneously went to zero SWE. At the very end of the melt season, the SWE that remained was a very small percentage of initial SWE, and it was distributed over a very small portion of basin area, as was seen in Figure 7.10.

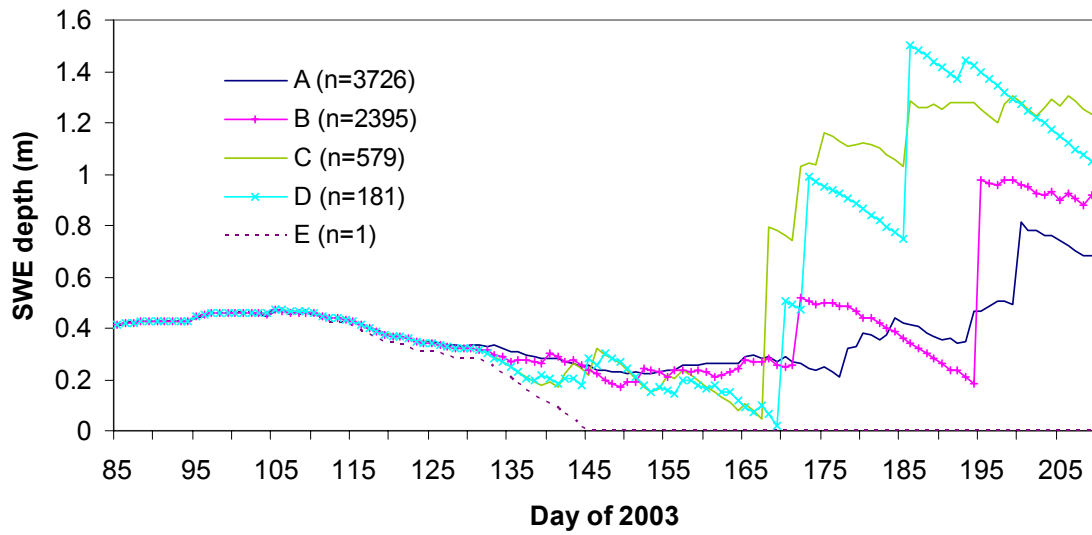


Figure 7.10. Average SWE depth across total basin area that is snow-covered in St. Louis Creek for the period of 26 March through 28 July, 2003. “n” is number of polygons in each simulation, A-E.

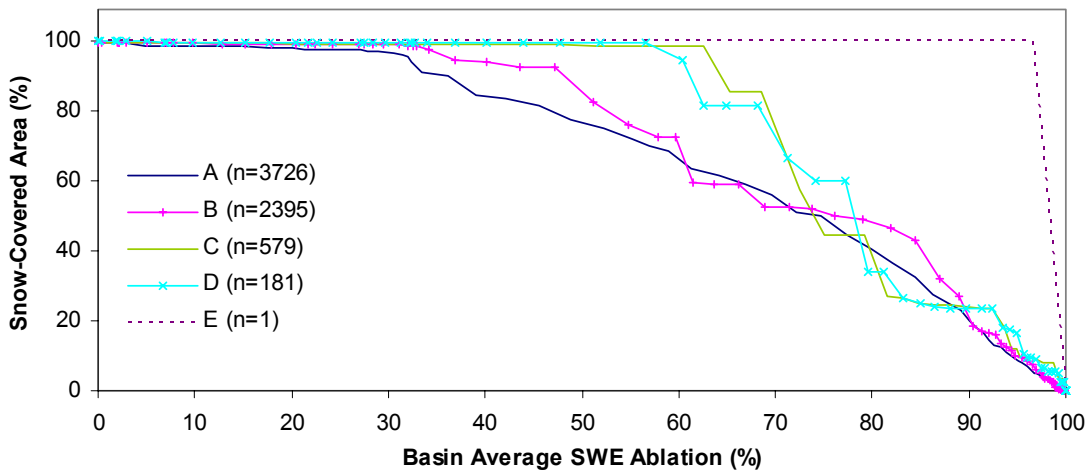


Figure 7.11. Relationship between basin snow-covered area and the progression of SWE depletion over St. Louis Creek from 26 March through 29 July, 2003.

Overall, the results for SCA depletion indicate that the model is sensitive to the distribution of initial SWE and the size and number of modeling units throughout the

basin when predicting snow-covered area depletion, even though the model is not sensitive to basin-average SWE. The implications of this are such that for modeling applications where the timing of snow-free area is of concern (e.g. ecological or atmospheric modeling), the way in which the basin is divided into modeling units may be of extreme importance. However, for hydrologic applications concerned with the total amount of water in the basin, the distribution of modeling units, for this particular set of circumstances, has little effect on the rate and timing of average basin SWE depletion and meltwater generation.

7.2.3 BASIN AVERAGE TEMPERATURE

Temperature results are shown in Figure 7.12. There was very little difference in daily average basin-wide temperature over the five simulations due to the fact that temperatures were determined in MicroMet as a function of elevation and lapse rate, and when all elevations were combined to produce average basin temperature the highs and lows canceled each other out. Although temperature differences between polygons are not shown in Figure 7.12, the increase in basin-average temperature throughout the melt season is well represented by MicroMet.

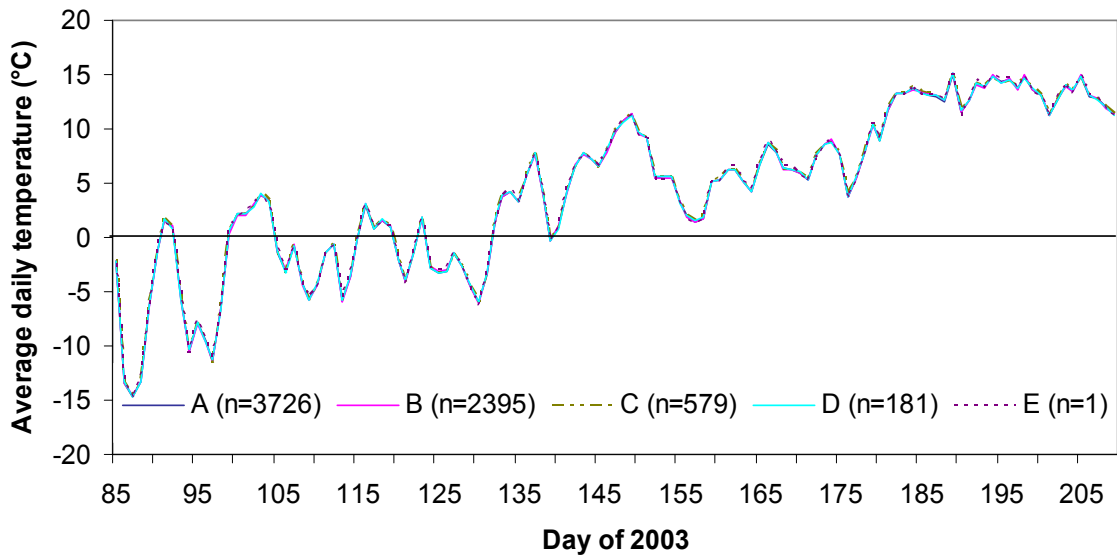


Figure 7.12. Average daily temperature averaged over St. Louis Creek basin for each simulation (A-E) for the modeling period 26 March through 28 July, 2003. “n” is the number of polygons in each simulation.

7.2.4 ST. LOUIS CREEK RUNOFF

SCA depletion was compared to reconstructed St. Louis Creek runoff using historical data from both East St. Louis Creek and Fool Creek (Figures 7.13 and 7.14). These charts imply that before 20% of the seasonal snowmelt runoff peak has passed, SnowModel predicted over 60% of the basin to be snow-free in all simulations. Love (1960), in a study of snow cover depletion and runoff in the Fraser Experimental Forest, found that in 1950 the spring runoff peak occurred when approximately half of the snow had disappeared, and when 80% of the snow was gone, the stream was declining in flow. The total spring/summer runoff for 1950 and 2003 were similar, with 2003 being slightly greater: East St. Louis discharge in 1950 was 93% of that in 2003 and Fool Creek 1950 discharge was 83% of 2003 discharge. Both years were very close to the average for pre-diversion flow in East St. Louis and Fool Creek. Therefore, it is possible

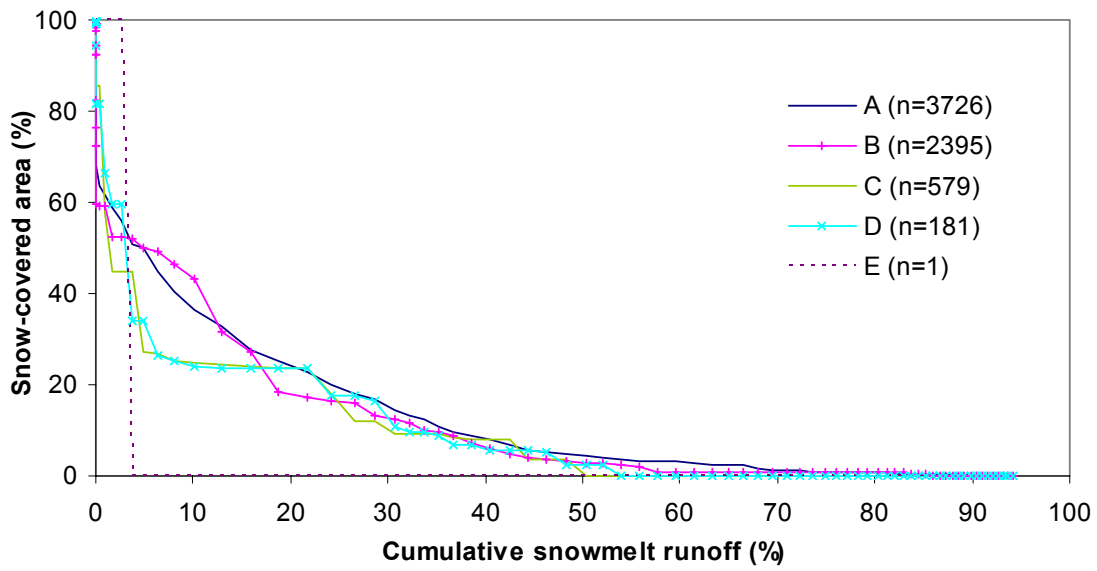


Figure 7.13. 2003 St. Louis Creek predicted snow covered area depletion related to cumulative snowmelt runoff, predicted using East St. Louis Creek data, in percent of seasonal total for simulations A through E.

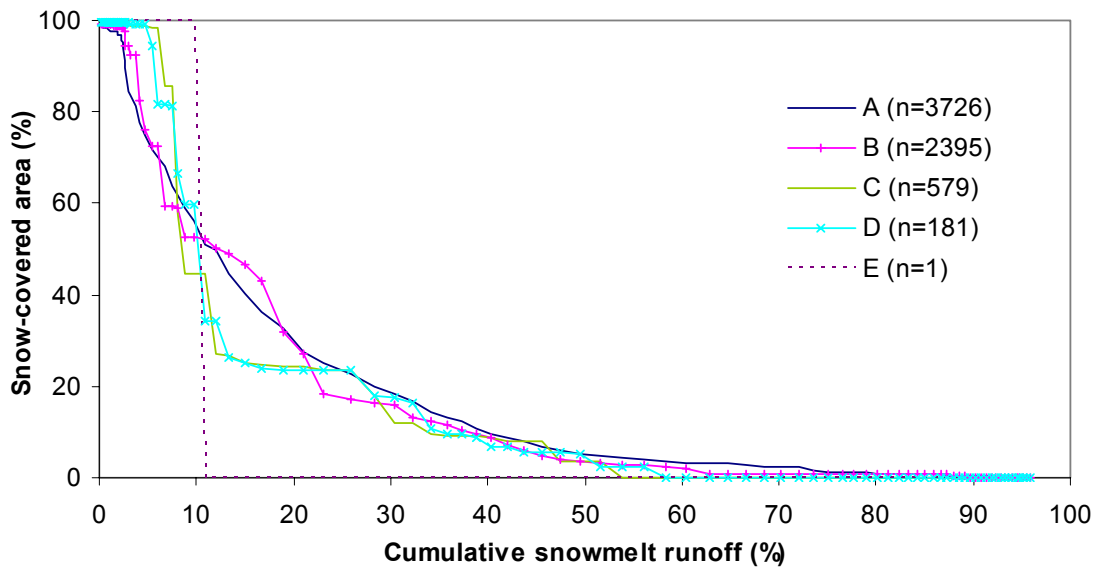


Figure 7.14. 2003 St. Louis Creek predicted snow covered area depletion related to cumulative snowmelt runoff, predicted using Fool Creek data, in percent of seasonal total for simulations A through E.

that the depletion curves for those two years could be somewhat similar. These results suggest that SnowModel likely predicted early meltout for St. Louis Creek basin in 2003.

7.2.5 SNOWMODEL RUNOFF

Daily runoff was calculated from cumulative runoff and a 15-day running mean was applied to the results (after Liston and Elder (2006a)) to improve visibility (Figure 7.15). St. Louis Creek runoff reconstructed using historical data from both Fool Creek and East St. Louis Creek are also shown in Figure 7.15. These results suggest that the amount of runoff calculated by SnowModel was clearly an overestimate of actual basin runoff, despite uncertainties in reconstructed St. Louis Creek discharge. Since SnowModel does not account for soil moisture recharge, it was anticipated that the magnitude and timing of runoff would not directly coincide with reconstructed runoff. The magnitude of cumulative daily runoff calculated by SnowModel for simulation A was 5.3 times greater than the magnitude of reconstructed cumulative daily runoff for St. Louis Creek using Fool Creek (FC), and 6.5 times greater than reconstructed cumulative daily runoff using East St. Louis Creek (ESL). The rising limb of the SnowModel runoff hydrograph started approximately 35 days prior to the inception of runoff from St. Louis Creek. However, the duration of both the SnowModel hydrograph peak and the St. Louis hydrograph peak was approximately 70 days. Although the timing and magnitude of runoff from SnowModel was not accurate, these results suggest that having a similar duration of runoff may indicate that SnowModel accurately depicted the spatial variability of melt in the basin, beginning with melt in low elevations and approximately 70 days later ending with melt in the highest elevations and most northerly aspects of the

basin. It is possible that accounting for timing and magnitude of soil moisture recharge would correct the runoff problem in SnowModel. However, the excessive magnitude of runoff may indicate that the problem is not entirely attributable to soil moisture recharge, but rather to an overestimation of incoming precipitation. The abrupt rise in SnowModel-predicted St. Louis Creek runoff beginning on day 188 is a result of overestimated predicted precipitation.

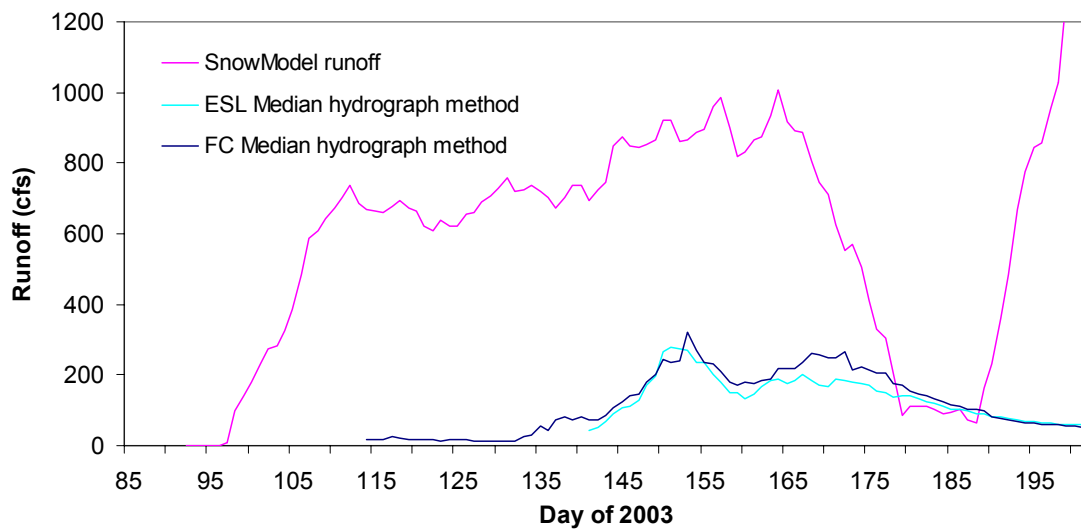


Figure 7.15. SnowModel daily runoff for St. Louis Creek basin, 26 March through 30 July, 2003, calculated using a 15-day moving average for visibility improvement. Also shown is St. Louis Creek runoff reconstructed from East St. Louis and Fool Creek historical runoff. The abrupt rise in SnowModel-predicted runoff beginning on day 188 is the result of excessive predicted incoming precipitation.

The cumulative runoff results presented in Figure 7.16 also suggest that the overestimation of runoff may be attributed to an overestimation of incoming precipitation. SnowModel cumulative runoff results for simulations A and D are shown in Figure 7.16. Simulations A and D were chosen for display because they are representative of the fine and coarse spatial modeling scale. For reference, mean basin SWE is also shown in Figure 7.16 for simulations A and D. Snowmelt runoff ceased around day 167 where the cumulative graph flattens out and SWE is 99% melted out

(Figure 7.7). Runoff after day 167 was attributed to incoming precipitation. Through the end of snowmelt, SnowModel predicted approximately 1.6 meters of cumulative runoff even though maximum basin average SWE was only 0.5 meters. A comparison was conducted between distributed SnowModel predicted precipitation input and St. Louis Creek and Fool Creek observed precipitation to investigate how well SnowModel (MicroMet) predicted incoming precipitation relative to observed at those two sites (refer to section 7.3.1). Precipitation records from Fool Creek and Fraser Headquarters show that an average of 0.25 meters of precipitation fell between the beginning of the modeling period (day 86) and the complete ablation of basin SWE (day 167), not 1.1 meters as predicted by MicroMet.

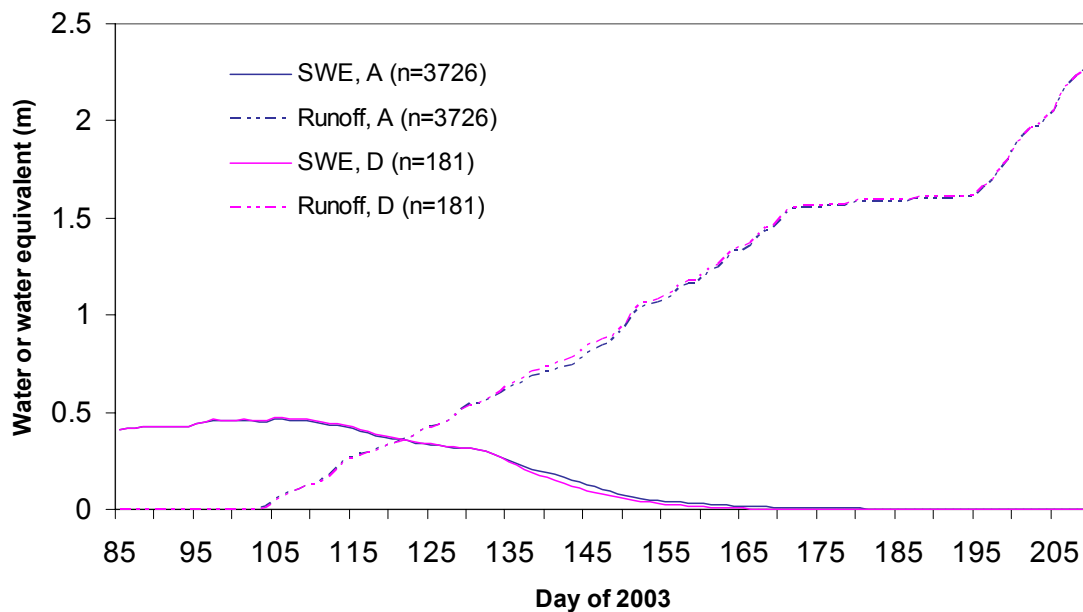


Figure 7.16. Mean basin SWE depletion and cumulative runoff for simulations A and D, 26 March through 30 July, 2003.

7.3. COMPARISON OF POLYGON RESULTS TO METEOROLOGICAL TOWER DATA

7.3.1 PRECIPITATION

A check on SnowModel precipitation input was conducted by comparing hourly MicroMet output for the simulation A polygons containing the Fool Creek rain gauge and the Fraser Headquarters rain gauge to the hourly observed data from the gauges. Cumulative precipitation for the polygons and the gauges is shown in Figure 7.17 and these results indicate that MicroMet clearly overestimated precipitation in these polygons. If these polygons are representative of MicroMet predicted precipitation across the basin, the excess precipitation could be a major contributing factor in the overestimation of runoff over the entire basin.

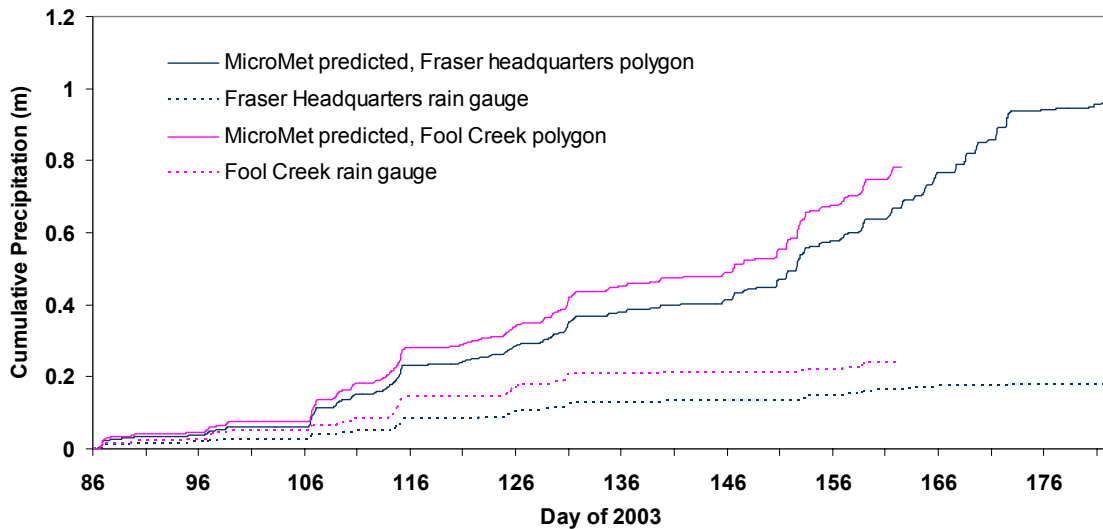


Figure 7.17. Cumulative precipitation comparison between the Fraser Headquarter rain gauge, the Fool Creek rain gauge and the MicroMet output precipitation for the polygons containing each rain gauge, 26 March through 1 August, 2003.

7.3.2 AIR TEMPERATURE

Air temperature observed at the Fool Creek tower and that predicted by MicroMet is shown in Figure 7.18, with a 12-hour moving average applied for clarity. Results comparing the St. Louis Creek tower observations to MicroMet-predicted air temperature in the Fraser Headquarters polygon were similar to those from Fool Creek (not shown). The air temperature predicted by MicroMet does not reflect the same extremes of high and low air temperature that were observed. The implication of not capturing extremes in snowpack temperature variability may be that the modeled snowpack assumes less energy is required to heat or cool the pack than would be required in reality. Missing temperature extremes is especially important if a melting snowpack freezes at night and requires energy to warm it before melt can take place, whereas the model may not cool the snowpack enough to refreeze it during the night, leading to overestimated melt during the day (e.g. 117, 118, 120 and 140).

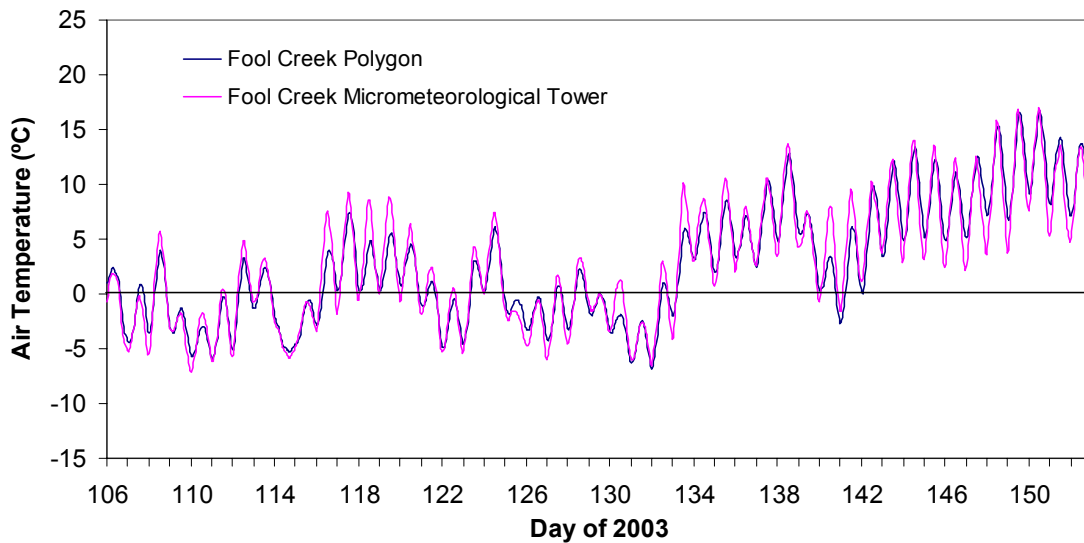


Figure 7.18. Air temperature observed at the Fool Creek meteorological tower and air temperature estimated by MicroMet for the polygon containing the Fool Creek meteorological tower. A 12-hour moving average was applied to improve clarity.

7.3.3 RADIATION

Observed incoming shortwave radiation at the Fool Creek meteorological tower and MicroMet simulated incoming shortwave radiation over the Fool Creek polygon are shown in Figure 7.19. Observed incoming radiation near the snow surface at the tower site was much greater than simulated incoming shortwave radiation under the canopy, as anticipated. Results and observations were similar for the St. Louis Creek tower and the Fraser headquarters polygon (not shown).

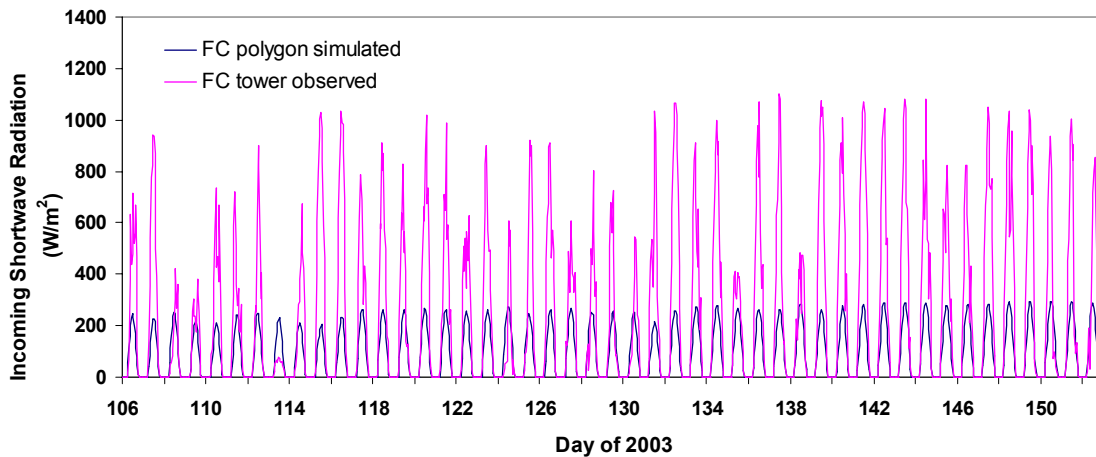


Figure 7.19. Observed incoming shortwave radiation at the Fool Creek meteorological tower and MicroMet simulated net shortwave radiation over the Fool Creek polygon containing the Fool Creek meteorological tower, 16 April through 2 June, 2003.

Observed and simulated incoming longwave radiation at the Fool Creek tower and Fool Creek polygon, respectively, is shown in Figure 7.20. Differences in incoming longwave radiation between the tower site and the forested polygon are likely due to the model accounting for longwave radiation emitted from the forest canopy and the model's estimation of incoming longwave as a function of air temperature and relative humidity.

Conditions were similar for the St. Louis tower site and simulated Fraser headquarters polygon (not shown).

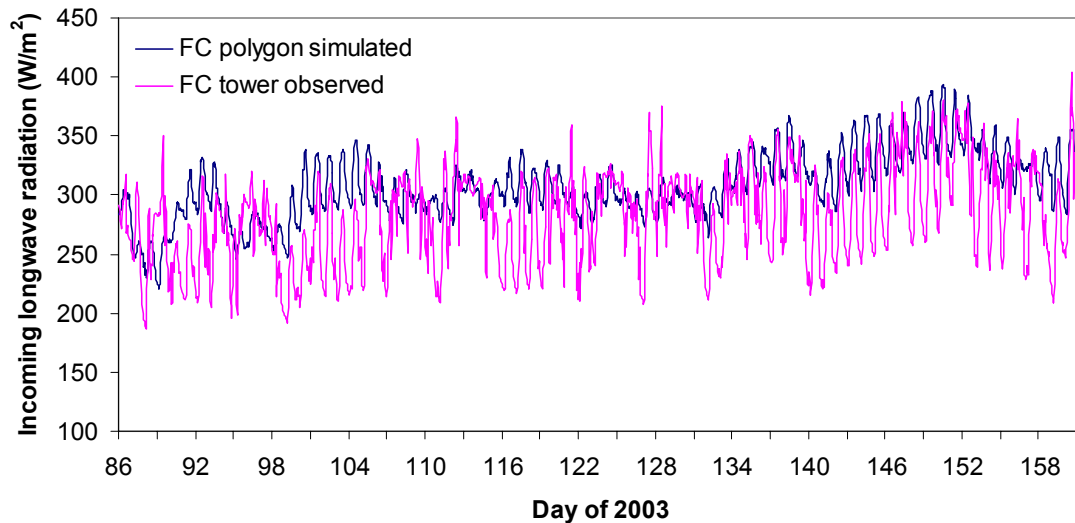


Figure 7.20. Observed incoming longwave radiation at the Fool Creek meteorological tower and MicroMet simulated net longwave radiation over the Fool Creek polygon containing the Fool Creek meteorological tower.

7.4 PRECIPITATION CORRECTION

Since incoming precipitation was overpredicted by MicroMet, a precipitation correction was applied by replacing LAPS precipitation estimates with observations from three precipitation gauges in the basin. In addition to using data from the Fool Creek and Fraser Headquarters rain gauges, data from the Upper Fool Creek rain gauge were used. The Upper Fool Creek gauge is located approximately 500 m uphill of the Fool Creek meteorological tower.

Comparisons of “corrected” MicroMet precipitation predictions are shown in Figure 7.21 along with observed precipitation at Fool Creek. The original precipitation

predicted by MicroMet is also shown to highlight the improvements made by using observed precipitation. Results were similar for St. Louis Creek precipitation (not shown).

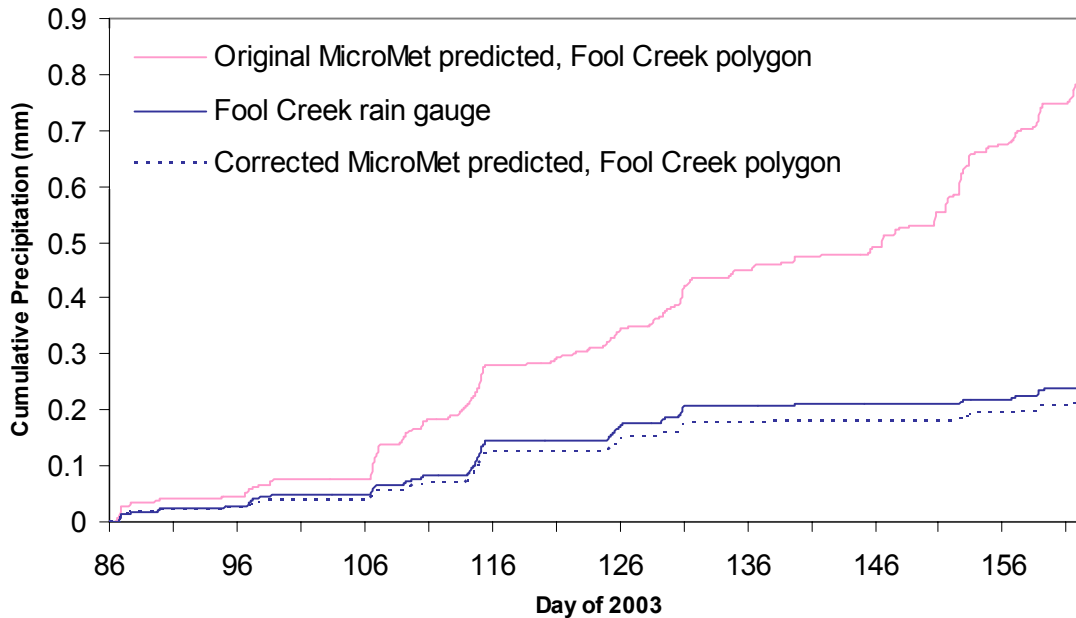


Figure 7.21. Precipitation measured at the Fool Creek precipitation gauge, precipitation predicted by MicroMet for the Fool Creek polygon using only LAPS data (original), and precipitation predicted by MicroMet for the Fool Creek polygon using observed precipitation (corrected).

Simulations A and D were run using new precipitation data, and the resulting basin-average SWE is shown in Figure 7.22 and SCA depletion is shown in Figure 7.23. The uncorrected basin-average SWE and SCA depletion curves are shown for comparison. No other meteorological parameters were altered in MicroMet, so the energy available for melt at each timestep was the same as in the original simulations. Simulations A and D were chosen to represent the fine and coarse resolutions, respectively. Using observed precipitation in MicroMet slightly decreased basin-average

SWE results, particularly early in the season, and slightly decreased SCA results. With less incoming precipitation, less SWE is accumulated in the basin, particularly between days 85 - 115. However, later in the melt season, differences in SWE are minimal, and this is reflected by minimal change in SCA depletion timing between the original and corrected simulations.

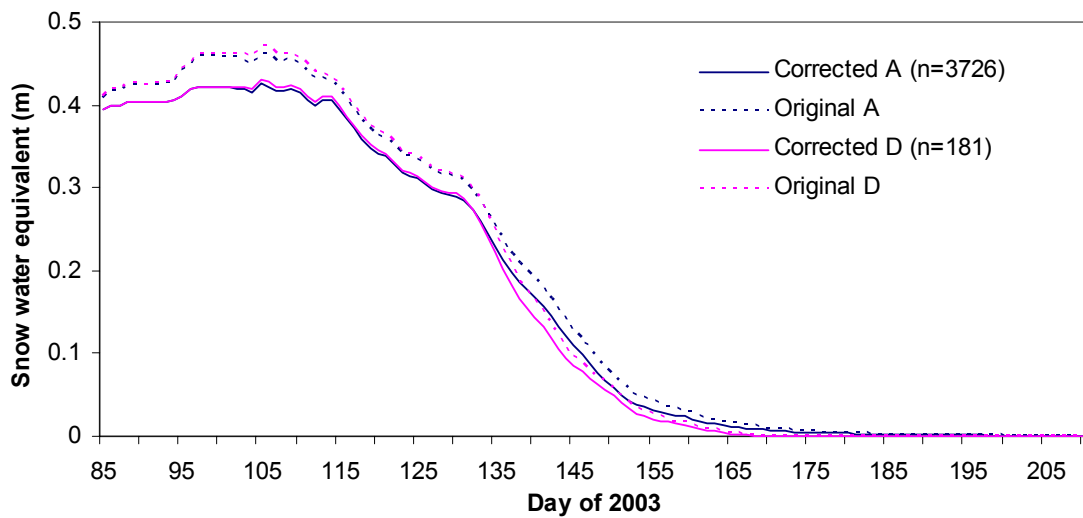


Figure 7.22. Precipitation-corrected and original basin-average snow water equivalent results for simulations A and D.

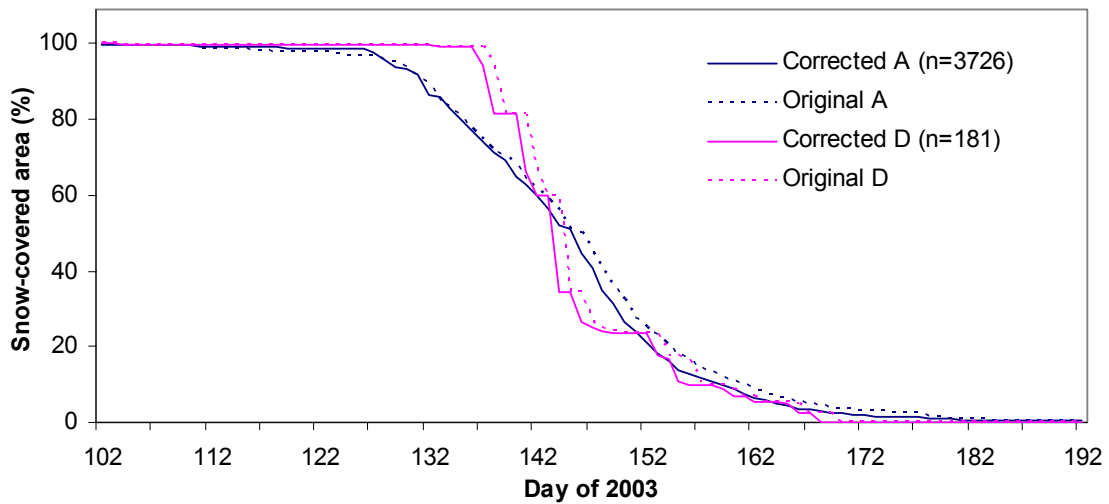


Figure 7.23. Precipitation-corrected and original snow-covered area results for simulations A and D.

Precipitation-corrected results for basin runoff are shown in Figure 7.24. As anticipated, reducing the amount of incoming precipitation reduced predicted runoff. Overall, the average incoming precipitation in the basin from the three precipitation gauges was 0.25 m over the modeling period. The initial basin-wide SWE for both simulations A and D was 0.39 m. Average precipitation plus average initial SWE was 0.65 m. The sum of precipitation and initial SWE should approximate runoff, since very little static snow sublimation or interception was calculated in SnowModel for the modeling period (not shown). Average basin runoff for corrected simulations A and D was 0.66 m compared to the unrealistic sum of the original precipitation and initial SWE, which was greater than 2.5 m.

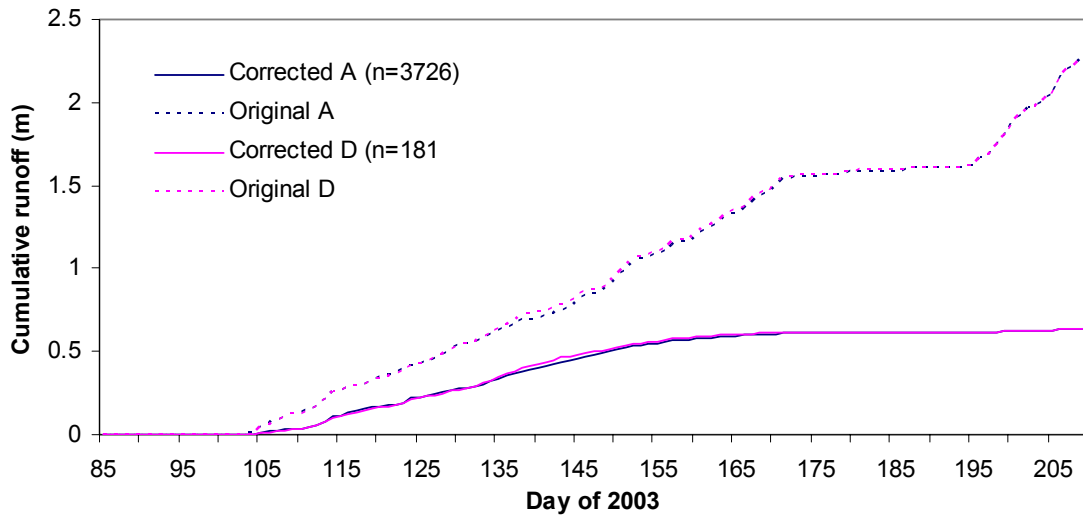


Figure 7.24. Original SnowModel-predicted St. Louis Creek basin runoff and precipitation-corrected predicted runoff for simulations A and D.

CHAPTER 8. CONCLUSIONS

The first objective of this study was to evaluate the performance of Fast All-Season Soil Strength (FASST) and SnowModel in estimating snowpack depletion at two mid-latitude sub-alpine sites in the Fraser Experimental Forest. Both FASST and SnowModel successfully predicted the magnitude and timing of snow depth depletion at both sites. Slight differences between FASST and SnowModel predictions were attributed to differences between how each model calculates snow pack physical properties such as snow metamorphism, albedo and new snow density. Differences in snow water equivalent predictions were attributed to differences in the way each model calculates new snow density and changes in snowpack density due to compaction from overburden, snow metamorphism and snowmelt.

The second objective of this project was to use SnowModel to simulate snow cover depletion in St. Louis Creek basin at varying spatial resolutions of hydrologic response units (HRUs). HRUs were created based on factors most affecting snow cover depletion rate and timing in St. Louis Creek basin: slope, aspect, elevation and vegetation cover. Five simulations were completed, with the finest resolution simulation having 3726 HRUs and the coarsest having one polygon representing the basin as a whole. It was found that the finer resolutions of modeling units were better able to represent the extreme spatial heterogeneity of snowpack depletion rate and timing in St. Louis Creek

basin. The coarser resolution simulations produced less realistic snowpack depletion rates and timing through a shorter melt season and simultaneous disappearance of snow covering large areas in the basin.

The final objective of this study was to compare snowpack depletion and runoff simulated using SnowModel to discharge from St. Louis Creek. Since St. Louis Creek is diverted above the stream gauge, 2003 discharge was estimated using pre-diversion (1943 – 1955) statistical relationships between St. Louis Creek and two smaller creeks within the basin. Snow-covered area depletion curves generated from five SnowModel simulations were compared to reconstructed runoff and it was determined that SnowModel likely predicted early snowpack depletion in the basin. SnowModel predicted that over 60% of the snow cover disappeared before even 20% of St. Louis Creek snowmelt runoff had occurred. The timing and magnitude of runoff predicted using SnowModel was compared to St. Louis Creek runoff, and the timing of predicted runoff was earlier than observed due to SnowModel's inability to account for soil moisture recharge. The lack of soil moisture accounting also contributed to an overestimation of runoff magnitude but the majority of the runoff overestimate was a result of errors in modeled incoming precipitation predicted by MicroMet. Errors in precipitation estimates were corrected by using observations from three precipitation gauges within the basin.

Overall, it was determined that when using these modeling units within St. Louis Creek basin the model is not sensitive to varying distributions when predicting overall basin-average SWE depletion, but that it is sensitive when predicting snow-covered area depletion. Therefore, for modeling applications such as hydrological modeling, where the

amount and timing of basin-wide SWE depletion is of interest, the division of modeling units is less important. However, for applications such as ecological or atmospheric modeling, when the extent, timing and duration of snow-free area are of interest, the division of modeling units is important.

SnowModel is a very useful tool for simulating snow cover depletion at varying spatial scales. However, adjustments could be made to better parameterize the model to St. Louis Creek basin. In order to better account for runoff timing and magnitude, it is recommended that a soil moisture recharge module be included in the SnowModel suite.

9. REFERENCES

- Alexander, R., Troendle, C., Kaufmann, M., Shepperd, W., Crouch, G. and Watkins, R., 1985. The Fraser Experimental Forest, Colorado: Research program and published research 1937-1985. Gen. Tech. Rep. RMRS-GTR-118. Fort Collins, CO: U.S. Department of Agriculture, Forest Service, Rocky Mountain Range and Experiment Station, pp. 35.
- Anderson, E.A., 1973. National Weather Service River Forecast System--Snow Accumulation and Ablation Model. Technical Memorandum NWS Hydro-17, pp. 217.
- Anderson, E.A., 1976. A point energy and mass balance model of a snow cover. NOAA Technical Report NWS-19.
- Baral, D. and Gupta, R., 1997. Integration of satellite sensor data with DEM for the study of snow cover distribution and depletion pattern. *Int. J. Remote Sensing*, 18(18): 3889-3894.
- Battaglin, W., Kuhn, G. and Parker, R., 1996. Using GIS to link digital spatial data and the Precipitation Runoff Modeling System: Gunnison River Basin, Colorado. In: M.F. Goodchild (Editor), *GIS and Environmental Modeling*. Oxford University Press, New York, pp. 123-128.
- Becker, A. and Braun, P., 1999. Disaggregation, aggregation and spatial scaling in hydrological modelling. *Journal of Hydrology*, 217(3-4): 239-252.
- Blöschl, G., Kirnbauer, R. and Gutknecht, D., 1991. Distributed snowmelt simulations in an alpine catchment 1. Model evaluation on the basis of snow cover patterns. *Water Resources Research*, 27(12): 3171-3179.
- Brazanec, W.A., 2005. M.S. Thesis. Evaluation of ultrasonic snow depth sensors for Automated Surface Observing System (ASOS). Department of Rangeland, Forest and Watershed Stewardship, Colorado State University, Fort Collins, 124 pp.

- Buttle, J.M. and McDonnell, J.J., 1987. Modeling the areal depletion of snowcover in a forested catchment. *Journal of Hydrology*, 90(1-2): 43-60.
- Carlson, N., 2006. Personal communication. Denver Water, Denver, Colorado.
- Charbonneau, R., Lardeau, J.P. and Obled, C., 1981. Problems of modeling a high mountainous drainage-basin with predominant snow yields. *Hydrological Sciences Bulletin*, 26(4): 345-361.
- Cline, D., Elder, K. and Bales, R., 1998. Scale effects in a distributed snow water equivalence and snowmelt model for mountain basins. *Hydrological Processes*, 12(10-11): 1527-1536.
- Cline, D., Elder, K., Davis, R.E., Hardy, J., Liston, G.E., Imel, D., Yueh, S.H., Gasiewski, A.J., Koh, G., Armstrong, R.L. and Parsons, M., 2003. Overview of the NASA Cold Land Processes Field Experiment (CLPX-2002). *Proceedings of Society of Photo-Optical Instrumentation Engineers*, 4894: 361-372.
- Doesken, N.J. and Judson, A., 1997. *The snow booklet: A guide to the science, climatology, and measurement of snow in the United States*. Colorado Climate Center, Department of Atmospheric Science, Colorado State University, Fort Collins, Colorado, 86 pp.
- Douville, H., Royer, J.-F. and Mahfouf, J.-F., 1995. A new snow parameterization for the Meteo-France climate model. Part 1: Validation in stand alone experiments. *Climate Dynamics*, 12(1): 21-35.
- Dunford, E.G. and Love, L.D., 1952. *The Fraser Experimental Forest, its work and aims*. U.S. Forest Service, Rocky Mountain Forest and Range Experiment Station. Station Paper 8, pp. 27.
- Dunne, T. and Leopold, L., 1978. *Water in Environmental Planning*. W. H. Freeman and Company, New York, 818 pp.
- Elder, K., 2006. *Fraser Experimental Forest East St. Louis Creek and Lower Fool Creek Daily Streamflow Data: 1941-1985*. U.S. Department of Agriculture, Forest Service, Rocky Mountain Research Station, Fort Collins, CO.
http://www.fs.fed.us/rm/data_archive. [March, 2006].

- Elder, K., Dozier, J. and Michaelsen, J., 1991. Snow accumulation and distribution in an alpine watershed. *Water Resources Research*, 27(7): 1541-1552.
- Elder, K. and Goodbody, A., 2004. CLPX-Ground: ISA Main Meteorological Data. Boulder, Colorado: National Snow and Ice Data Center. Digital Media.
- Famiglietti, J.S. and Wood, E.F., 1995. Effects of spatial variability and scale on areally averaged evapotranspiration. *Water Resources Research*, 31(3): 699-712.
- Fassnacht, S.R., 2004. Estimating Alter-shielded gauge snowfall undercatch, snowpack sublimation, and blowing snow transport at six sites in the conterminous United States, 61st Eastern Snow Conference, Portland, Maine, pp. 15-26.
- Flügel, W.-A., 1995. Delineating hydrological response units by Geographical Information System analyses for regional hydrological modelling using PRMS/MMS in the drainage basin of the River Bröl, Germany. *Hydrological Processes*, 9: 423-436.
- Frankenstein, S. and Koenig, G., 2004. Fast All-season Soil STrength (FASST). Cold Regions Research and Engineering Laboratory, US Army Corps of Engineers, pp. 86.
- Frankenstein, S., Sawyer, A. and Koeberle, J., 2007. Comparison of FASST and SNTHERM in three snow accumulation regimes. *Journal of Hydrometeorology*, in review.
- Goodison, B.E., 1978. Accuracy of Canadian snow gage measurements. *Journal of Applied Meteorology*, 17: 1542-1548.
- Gurtz, J., Baltensweiler, A. and Lang, H., 1999. Spatially distributed hydrotope-based modelling of evapotranspiration and runoff in mountainous basins. *Hydrological Processes*, 13: 2751-2768.
- Hardy, J.P., Davis, R.E., Jordan, R., Li, X., Woodcock, C., Ni, W. and McKenzie, J.C., 1997. Snow ablation modeling at the stand scale in a boreal jack pine forest. *Journal of Geophysical Research-Atmospheres*, 102(D24): 29397-29405.

- Harrington, R., Elder, K. and Bales, R., 1995. Distributed snowmelt modeling using a clustering algorithm. In: W.M. Tonnessen K., and Tranter M. (Editor), Biogeochemistry of Seasonally Snow-Covered Catchments. IAHS, Proc. Boulder Symp., pp. 167-174.
- Hendrick, R., Filgate, B. and Adams, W., 1971. Application of environmental analysis to watershed snowmelt. *Journal of Applied Meteorology*, 10: 418-429.
- Holcombe, J., 2004. M.S. Thesis. A modeling approach to estimating snow cover depletion and soil moisture recharge in a semi-arid climate at two NASA CLPX sites, Department of Forestry, Rangeland and Watershed Stewardship, Colorado State University, Fort Collins, Colorado, 102 pp.
- Jordan, R., 1991. A one-dimensional temperature model for snow cover, Technical Documentation for SN THERM.89. U.S. Army Cold Regions Research and Engineering Laboratory, pp. Special Report 657.
- Jordan, R.E., Andreas, E.L. and Makshtas, A.P., 1999. Heat budget of snow-covered sea ice at North Pole 4. *Journal of Geophysical Research*, 104(C4): 7785-7806.
- Kirnbauer, R., Blöschl, G. and Gutknecht, D., 1994. Entering the era of distributed snow models. *Nordic Hydrology*, 25(1-2): 1-24.
- Kite, G.W. and Kouwen, N., 1992. Watershed modeling using land classifications. *Water Resources Research*, 28(12): 3193-3200.
- Kouwen, N., Soulis, E.D., Pietroniro, A., Donald, J. and Harrington, R.A., 1993. Grouped response units for distributed hydrologic modeling. *Journal of Water Resources Planning and Management*, 119(3): 289-305.
- Leaf, C.F., 1969. Aerial photographs for operational streamflow forecasting in the Colorado Rockies, Western Snow Conference, Salt Lake City, pp. 19-28.
- Leavesley, G. and Stannard, L., 1990. Application of remotely sensed data in a distributed-parameter watershed model, Proceedings of the Workshop on Applications of Remote Sensing in Hydrology, Saskatoon, Sask., pp. 47-68.
- Link, T. and Marks, D., 1999. Distributed simulation of snowcover mass- and energy-balance in the boreal forest. *Hydrological Processes*, 13(14-15): 2439-2452.

- Liston, G.E., 1995. Local advection of momentum, heat and moisture during the melt of patchy snow covers. *Journal of Applied Meteorology*, 34: 1705-1717.
- Liston, G.E., 1999. Interrelationships among snow distribution, snowmelt and snow cover depletion: Implications for atmospheric, hydrologic, and ecologic modeling. *Journal of Applied Meteorology*, 38: 1474-1487.
- Liston, G.E. and Elder, K., 2006a. A distributed snow-evolution modeling system (SnowModel). *Journal of Hydrometeorology*, 3: 524-538.
- Liston, G.E. and Elder, K., 2006b. A meteorological distribution system for high-resolution terrestrial modeling (MicroMet). *Journal of Hydrometeorology*, 7: 217 - 234.
- Liston, G.E., Haehnel, R.B., Sturm, M., Hiemstra, C.A., Berezovskaya, S. and Tabler, R.D., 2006. Simulating Complex Snow Distributions in Windy Environments using SnowTran-3D. Submitted to *Journal of Glaciology*.
- Liston, G.E. and Hall, D.K., 1995. An energy-balance model of lake-ice evolution. *Journal of Glaciology*, 41(138): 373-382.
- Liston, G.E. and Hiemstra, C.A., 2006. A simple snow data assimilation system for complex snow distributions. *Journal of Hydrometeorology*, in review.
- Liston, G.E., Hiemstra, C.A., Elder, K. and Cline, D.W., 2007. Meso-cell study area (MSA) snow distributions for the Cold Land Processes Experiment (CLPX). in review.
- Liston, G.E. and Sturm, M., 1998. A snow-transport model for complex terrain. *Journal of Glaciology*, 44(148): 498-516.
- Liston, G.E., Winther, J.-G., Bruland, O., Elvehoy, H. and Sand, K., 1999. Below-surface ice melt on the coastal Antarctic ice sheet. *Journal of Glaciology*, 45(150): 273-285.
- Love, L.D., 1960. The Fraser Experimental Forest- Its work and aims. Res. Pap. RM-RP-8. Fort Collins, CO: US Department of Agriculture, Forest Service, Rocky Mountain Range and Experiment Station. 16 p.

- Luce, C.H. and Tarboton, D.G., 2004. The application of depletion curves for parameterization of subgrid variability of snow. *Hydrological Processes*, 18(8): 1409-1422.
- Luce, C.H., Tarboton, D.G. and Cooley, K.R., 1998. The influence of the spatial distribution of snow on basin-averaged snowmelt. *Hydrological Processes*, 12: 1671-1683.
- Male, D.H. and Granger, R.J., 1981. Snow surface-energy exchange. *Water Resources Research*, 17(3): 609-627.
- Male, D.H. and Gray, D.M., 1981. Snowcover ablation and runoff. In: D.M. Gray and D.H. Male (Editors), *Handbook of Snow*. The Blackburn Press, New Jersey, pp. 776.
- Martinec, J., 1985. Snowmelt runoff models for operational forecasts. *Nordic Hydrology*, 16: 129-136.
- Meek, D.W. and Hatfield, J.L., 1994. Data quality checking for single station meteorological databases. *Agricultural and Forest Meteorology*, 69: 85-109.
- Meiman, J.R., 1968. Snow accumulation related to elevation, aspect and forest canopy, Snow hydrology proceedings of the workshop seminar sponsored by Canadian National Committee for the International Hydrological Decade and the University of New Brunswick, pp. 35-47.
- Melloh, R.A., Hardy, J.P., Bailey, R.N. and Hall, T.J., 2002. An efficient snow albedo model for the open and sub-canopy, 59th Eastern Snow Conference, Stowe, VT, pp. 119-132.
- Metcalfe, R.A. and Buttle, J.M., 1995. Controls of canopy structure on snowmelt rates in the Boreal forest, Proceedings of 52nd Eastern Snow Conference, Toronto, Ontario, Canada, pp. 249-257.
- Pomeroy, J.W. and Dion, K., 1996. Winter radiation extinction and reflection in a boreal pine canopy: Measurements and modelling. *Hydrological Processes*, 10: 1591-1608.

- Porth, L., 2006. Personal communication. Statistician, US Forest Service, Rocky Mountain Research Station, Fort Collins, Colorado.
- Retzer, J.L., 1962. Soil Survey of Fraser Alpine Area, Colorado. U.S. Department of Agriculture in cooperation with Colorado Agricultural Experiment Station, pp. 47.
- Roesch, C.A., 2000. Assessment of the land surface scheme in climate models with focus on surface albedo and snow cover. Zurcher Klima-Schriften 78, ETH Geographisches Institut, Zurich.
- Thyer, M., Beckers, J., Spittlehouse, D., Alila, Y. and Winkler, R., 2004. Diagnosing a distributed hydrologic model for two high-elevation forested catchments based on detailed stand- and basin-scale data. Water Resources Research, 40(1).
- USACE, 1953. Snow investigations, Research Note 16, Snow-coverer depletion and runoff. U.S. Army Corps of Engineers, North Pacific Division, Portland, Oregon, pp. 64.
- USACE, 1956. Snow Hydrology, U. S. Army Corps of Engineers. Portland, Oregon, pp. 437.
- USGS, 2001. National Land Cover Dataset. <http://seamless.usgs.gov/website/seamless/products/nlcd01.asp>. August, 2005.
- USGS, 2006. Gauge data and station location. <http://waterdata.usgs.gov/co/nwis/sw>, September, 2005.
- USGS, 2006. National Elevation Dataset. <http://ned.usgs.gov/>. August, 2005.
- Viger, R.J., Markstrom, S.M., Leavesley, G.H. and Stewart, D.W., Undated. The GIS Weasel - An interface for the development of spatial parameters for physical process modeling, U.S. Geological Survey.
- Wood, E.F., Sivapalan, M., Beven, K. and Band, L., 1988. Effects of spatial variability and scale with implications to hydrologic modeling. Journal of Hydrology, 102(1-4): 29-47.

Yang, D., Kane, D.L., Hinzman, L.H., Goodison, B.E., Metcalfe, J.R., Louie, P.Y.T., Leavesley, G., Emerson, D.G. and Hanson, C.L., 2000. An evaluation of the Wyoming gauge system for snowfall measurement. *Water Resources Research*, 36(9): 2665-2677.